Quantified Carbon Dioxide Removal from an Alkalinity Addition Field Trial in the Kvina River, Norway

Isaac W. R. Bahler[1,2], Benjamin F. Trueman[2], Rolf D. Vogt[3], Jack R. Tucker[2], Catherine E. Brenan[2], Shannon M. Sterling[1,2]*

[1] Department of Earth and Environmental Sciences, Dalhousie University, 6287 Alumni Crescent, PO Box 15000, Halifax, Nova Scotia B3H 4R2, Canada

[2] CarbonRun, PO Box 14, 1 Research Drive, Dartmouth, Nova Scotia B2Y 4M9, Canada

[3] Norwegian Institute for Water Research (NIVA), Sognsveien 72, 0855 Oslo, Norway

* Corresponding Author: shannon.sterling@dal.ca

Submitted to Environmental Science & Technology: [August 4th, 2026]

ABSTRACT

River alkalinity enhancement (RAE) is a carbon dioxide removal (CDR) approach in which alkaline minerals are added to rivers to accelerate weathering reactions that neutralize acidity and increase alkalinity export to the ocean. Although river liming is widely used to mitigate acidification, it has not been quantified as a CDR approach. Here we report results from a 98-day RAE trial in the Kvina River, Norway, conducted within an existing liming programme. The trial increased the existing pH from 6.0 to 6.8 by adding an additional 1 480 t of calcite. CDR was quantified by comparing the increase in alkalinity export at the river mouth relative to a limed control site. The trial generated 250 ± 30 tonnes carbon dioxide equivalent (t CO_2e) of gross CDR, corresponding to a gross efficiency of 0.17 ± 0.02 t CO_2e per t calcite and 54 % of the theoretical maximum CDR. Apart from phosphate, no other nutrients, trace metals, or indicators of an adverse water-quality impact increased significantly. These findings provide field-scale evidence that modestly increasing pH targets at existing liming facilities can increase alkalinity export and generate quantifiable CDR under site-specific hydrological, feedstock, and lifecycle conditions.

KEYWORDS

River alkalinity enhancement (RAE); carbon dioxide removal (CDR); river liming; land-ocean-aquatic-continuum (LOAC); dissolved inorganic carbon (DIC); additionality; freshwater acidification; Atlantic salmon (*Salmo salar*).

INTRODUCTION

Meeting the 1.5–2 °C temperature goals of the Paris Agreement requires both deep emissions cuts and the rapid deployment of atmospheric carbon dioxide removal (CDR) approaches capable of generating durable negative emissions.[1–4] The urgent need for reliable approaches that can be scaled up to deliver gigaton-scale CDR has prompted a surge of interest in novel CDR pathways.[5,6] A promising set of CDR approaches focuses on alkalinity enhancement along the land-to-ocean aquatic continuum (LOAC), in which alkaline feedstocks are deployed to neutralize H^+ and leverage the ocean's dissolved inorganic carbon (DIC) reservoir to meet the millennial-scale storage requirement recognized as required for durable removals.[7–11] Such deployments include terrestrial-based approaches such as enhanced rock weathering (ERW)[12–14] and marine approaches such as ocean alkalinity enhancement (OAE).[15,16] A natural extension of these approaches is the development of river alkalinity enhancement (RAE), which has so far received relatively little study.

Rivers are the principal source of alkalinity to the oceans, exporting approximately 0.3–0.5 Pg C yr^{-1} as DIC, and therefore offer considerable potential to enhance oceanic alkalinity export through RAE.[17–20] Rivers also provide favourable conditions for alkaline feedstock dissolution. Their typically dilute waters remain undersaturated with respect to carbonate minerals such as calcite and dolomite[21], maintaining a strong dissolution gradient. At the same time, supersaturation of CO_2 supplies the carbonic acid required to drive carbonate dissolution[22], while high gas-exchange velocities may replenish the consumed CO_2 through atmospheric exchange.[23,24] Unlike terrestrial ERW or OAE, rivers provide a one-dimensional, generally well-mixed flow path in which dissolution, transport, and downstream dispersion occur within a

defined aquatic corridor. Thus, rivers enable CDR quantification via direct observation of reduced acidity export and increased alkalinity delivery to the ocean. Consequently, RAE occupies an intermediate position between terrestrial ERW and OAE: it combines the CO_2-rich, well-mixed conditions favourable for carbonate dissolution[25] with a constrained transport pathway that avoids both the high spatial variability complicating attribution in ERW[12,13,26,27] and the three-dimensional dilution that challenges monitoring in OAE.[28,29]

River alkalinity enhancement (RAE) works by adding alkaline minerals to river systems, where subsequent dissolution increases alkalinity and DIC flux to the ocean. When calcite dissolves via carbonic acid weathering,

$$CaCO_{3(s)} + CO_{2(aq)} + H_2O_{(l)} \rightarrow Ca^{2+}{}_{(aq)} + 2HCO_3^-{}_{(aq)} \quad (1)$$

It produces two equivalents of alkalinity representing two moles of DIC, one derived from aqueous CO_2 and one from the fossil C added by calcite (Equation 1). Depending on the final pH of the solution and continued acid inputs to the river, bicarbonate (HCO_3^-) may be either delivered to the ocean or protonated back to dissolved CO_2,

$$2HCO_3^-{}_{(aq)} + 2H^+{}_{(aq)} \rightarrow 2CO_{2\,(aq)} + 2H_2O_{(l)} \quad (2)$$

and, depending on the gas exchange velocity of the river, this CO_2 can subsequently evade to the atmosphere, reducing downstream DIC export. Calcite can also dissolve through acid neutralization reactions with non-carbonic acids, including strong mineral acids and weak natural organic acids,

$$CaCO_{3(s)} + 2H^+{}_{(aq)} \rightarrow Ca^{2+}{}_{(aq)} + CO_2\uparrow_{(g)} + H_2O_{(l)} \quad (3)$$

in which the feedstock carbon is released as fossil CO_2 and acidity that would otherwise have been exported downstream to the ocean is neutralized. This increases the alkalinity exported to the ocean by up to two equivalents per mole of calcite dissolved. Combining Equation 2 with Equation 1 yields the same net expression as Equation 3, supporting an increase of two equivalents of alkalinity and the emission of one mole of fossil CO_2. So, regardless of the reaction (Equations 1, 2 or 3 in combination), subsequent carbonate equilibration and CO_2 exchange determine the final partitioning between DIC and atmospheric CO_2.

Calcite added to the river may not all be transported to the ocean as dissolved alkalinity or DIC; it may settle to the river bottom, or undergo secondary precipitation, returning both DIC to the solid phase.[30–32] Below pH ~6.3, a larger fraction of DIC occurs as dissolved CO_2, increasing the risk of evasion (loss of CO_2 and DIC), though the magnitude depends on the extent of CO_2 supersaturation and river gas-transfer velocity. Organic-acid deprotonation can also convert bicarbonate to CO_2 and reduce DIC export, an effect enhanced as rising pH deprotonates more organic acids. Alkalinity loss can also arise if the organic-acid pool is mineralized, both in-river and in estuaries.[33] Improvements to quantification of in-river and estuarine loss processes are currently needed for both RAE and to test assumptions currently used in ERW deployments and to evaluate potential near-field coastal implications for OAE.[34,35]

Historically, long-range transported atmospheric deposition of strong sulphuric and nitric acids acidified catchments with low natural buffering capacity (e.g., Eastern Canada, Eastern USA and Scandinavia). Lowered pH along with mobile acid anions mobilized toxic aluminum species causing major declines in Atlantic salmon (*Salmo salar*) and sea trout (*Salmo trutta*).[36,37] To counteract acidification and associated salmonid losses, governments in affected regions

established large-scale liming programs in the 1970s and 1980s.[38,39] These programs applied finely ground alkaline minerals (generally calcite or dolomite) to rivers and lakes, and successfully increased pH and reduced the aluminum toxicity leading to salmonid population recovery.[37,38,40]

Liming programs have been assumed to act as a net source of CO_2 to the atmosphere[41] because reactions between acidity (strong or weak) and fossil carbon in the liming material release fossil CO_2 and the typical pH targets (6.0–6.4) promote bicarbonate reprotonation and CO_2 degassing.[36] However, despite the scale and longevity of these interventions, their implications for riverine carbon cycling have not previously been quantified.

Here we conduct a trial in the Kvina River using an existing liming facility to test whether increased calcite addition generates quantifiable CDR, and investigate the following research questions:

1. How much gross and net carbon removal (t CO_2e) was generated by adding additional calcite to the existing liming programme and with what efficiency?
2. What are the effects of adding additional calcite above conventional liming rates on river chemistry and environmental safety thresholds during the trial?

MATERIALS AND METHODS

Study Area

The Kvina River in Agder County, southern Norway, has a nival–pluvial hydrological regime with a mean annual discharge in the Kvina mainstem is ~24.6 m^3 s^{-1} draining an 809 km^2 Precambrian crystalline watershed with low natural buffering capacity (Table S1). A left-bank

tributary (Litleåne) joins the Kvina mainstem at the Kvinesdal Kommune, approximately 7 km upstream from the river mouth before discharging into the Fedafjord estuary on the North Sea coast (Figure 1a).

Historically, the Kvina supported abundant Atlantic salmon populations, but acidification lowered river pH to 4.5–5.2, which, along with elevated sulphate fluxes, increased labile aluminum and eliminated salmonid reproduction.[42] To restore the salmon populations, Norway's national acidification mitigation program installed liming infrastructure in the Kvina watershed beginning in the 1990s (Figure 1d). The Norwegian Environment Agency (Miljødirektoratet) sets pH targets for Kvina River that vary by season: pH 6.0 from June 1 to February 14 (259 days), pH 6.2 from February 15 to March 31 (45 days), and pH 6.4 from April 1 to May 31 (61 days), when sensitive salmon life stages coincide with acid pulses and elevated aluminum concentrations during spring snowmelt.[39,40] The Nyland dosing station (est. 2000) was built on the Kvina River mainstem, located 15.6 km from the river mouth (Figure 1b); this dosing station delivers finely ground calcite slurry (Omya Biokalk; 95 % $CaCO_3$, 2 % $MgCO_3$; D_{50} ~ 2 μm; C fraction 116 g kg^{-1}).[42] A second doser (Steindør) operates on the Litleåne tributary.

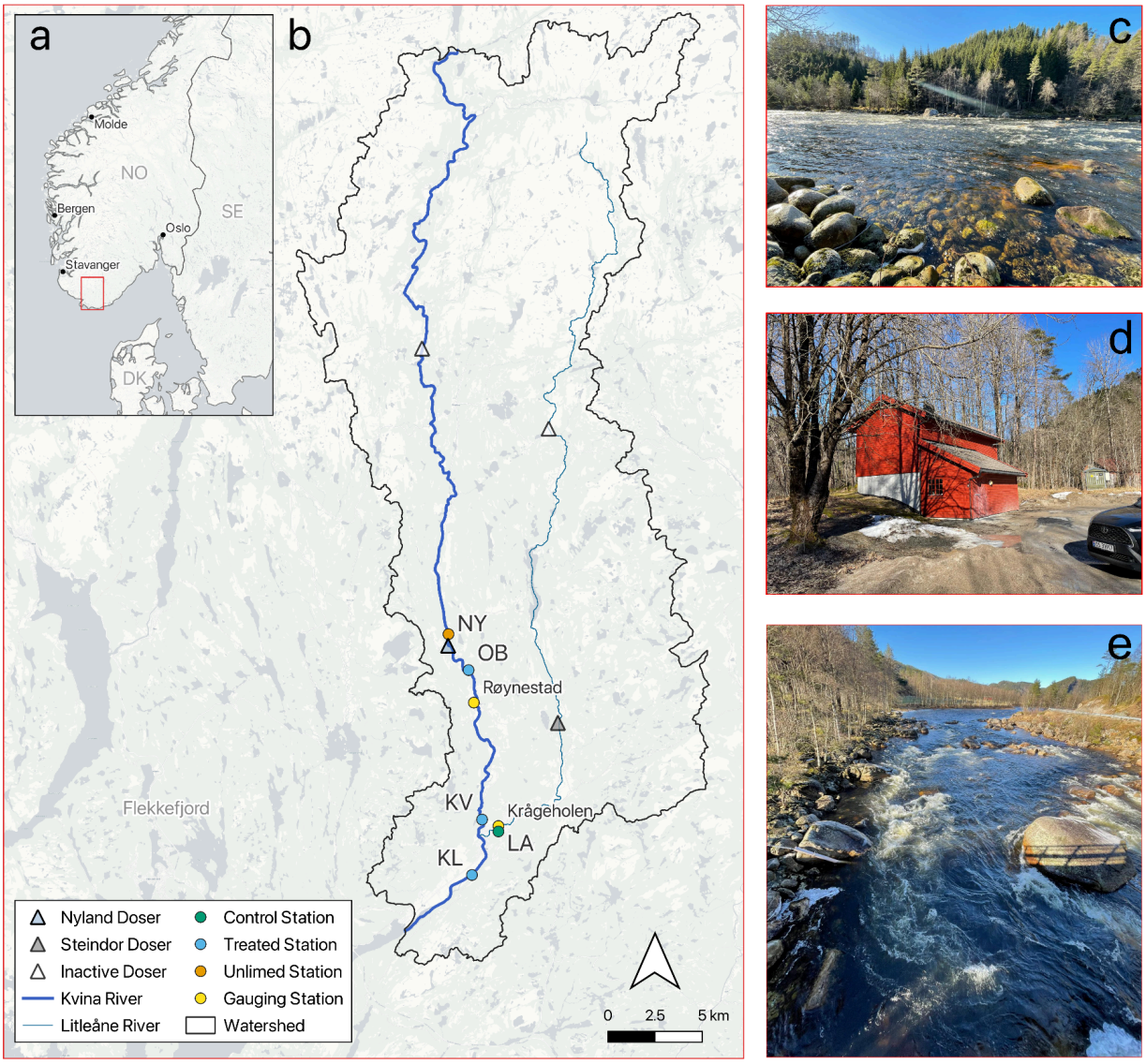

Figure 1. Kvina River and its monitoring and dosing sites: **(a)** Kvina River watershed location (red box) in Agder County, Norway and the calcite feedstock quarry in Molde; **(b)** The Kvina Watershed boundary (grey). Monitoring stations for this project are: Nyland (NY) 58.411°N, 6.929°E, Oksesteinbrua (OB) 58.396°N, 6.943°E, Litleåne (LA) 58.322°N, 6.974°E, Kvitla (KV) 58.326°N, 6.959°E and Klosters (KL) 58.299°N, 6.950°E; **(c)** Kvina River at the Nyland (NY) monitoring station; **(d)** Nyland Doser; **(e)** Oksesteinbrua (OB) monitoring station.

Experimental Design and Data Collection

The Kvina River Trial increased calcite addition rates at the Nyland doser to maintain an in-stream pH target of 7.0 for 98 days from June 10 to September 15, 2025, defining the CDR quantification period. We quantified the impact of the increased alkalinity addition by comparing two scenarios: the trial scenario, in which the pH target for the Nyland doser is increased to 7.0, and the counterfactual (*business as usual)* scenario, which represents conditions during the trial period if liming had not been increased. Calcite addition at the Steindør doser was unaffected by the trial, and therefore, observations from Litleåne før Kvina (LA) provided a limed control to characterize the counterfactual condition. Water chemistry and discharge at LA correlate well with those of the Kvina mainstem (Figure S1), justifying the use of LA in the counterfactual model. We use the term "additional" to represent the difference between the project and the counterfactual scenarios.

Data used to quantify the trial and counterfactual scenarios were collected across a monitoring network where stations were classified by liming status (limed or unlimed) and trial status (control or treatment; i.e., unaffected or affected by the intervention). Stations along the Kvina mainstem are (Figure 1): Nyland (NY, immediately above the Nyland doser serving as upstream unlimed control station); Oksesteinbrua (OB, limed treatment station, 2.27 km downstream of NY); Kvitla (KV, downstream of the doser beyond the weathering zone though upstream of the control tributary); Klosters (KL, limed treatment station at the river-mouth, serving as the CDR accounting point). To evaluate river chemistry changes, we compared physical and chemical observations between upstream (NY) and downstream (OB). We also evaluated trial period water chemistry at KL against a historic baseline (matched to the 98 days of the trial).

We deployed a combination of high-frequency in situ sensors and weekly grab sampling at four stations along the Kvina River (NY, OB, LA, KL). Weekly grab samples were collected and filtered[43] with a 0.45 μm mesh and analyzed by the Norwegian Institute for Water Research (NIVA) and ALS Global (ISO 17025) laboratories for total alkalinity (TA), acid neutralizing capacity (ANC), DIC, major ions, nutrients, DOC, aluminum, iron and trace metals (Table S2). Continuous *in situ* sensors recorded pH, pCO_2, temperature, and conductivity at 5–15-minute intervals. The pH and conductivity sensors were calibrated weekly following manufacturer protocols; pCO_2 was calibrated before the trial period (SI).[44] All sensors were inspected and cleaned weekly during field visits to reduce biofouling and sediment accumulation around the sensors.

Continuous discharge at the NY dosing station was measured directly from a stilling well using a stage–discharge rating curve developed from Norwegian Water Resources and Energy Directorate (NVE) streamflow data. Discharge at the river mouth was estimated using a linear scaling model based on partial watershed area that translated upstream discharge from Røynestad and NY gauges to KL.

Batch calcite dissolution kinetics were simulated in PHREEQC v3[45] incorporating average solution pH, alkalinity, temperature, and calcium concentration as well as calcite quantity (1.7×10^{-4} mol kg w^{-1}). Calcite was allowed to dissolve kinetically on a graded time-step schedule (Figure S2a). Two rate parameters, specific surface area ($1 \times 10^6 – 5 \times 10^6$ cm^2 mol^{-1}) and the saturation-state inhibition exponent γ (0.5 – 1), were propagated through a 1000-member Monte Carlo ensemble with uniformly distributed draws and mapped on a paired 10 × 10 sensitivity grid over the same ranges (Figure S2b).

CDR Quantification

We define Potential CDR as the theoretical maximum CDR for the trial, it is estimated by assuming complete dissolution of the total additional calcite and multiplying by the Feedstock $_{\text{CDR potential}}$. Potential CDR serves as an upper-bound reference: by assuming no decrease in reaction efficiency, it sets a ceiling that trial CDR is unlikely to reach (Table S5). Feedstock $_{\text{CDR potential}}$ is calculated from the composition of the feedstock using the adjusted Steinour equation[46], which sums the alkalinity-generating oxides (CaO, MgO, Na_2O, K_2O), subtracts the non-contributing (SO_4) or acid-producing components (P_2O_5), weights each term by its oxide molar mass, and scales the result by the molar mass of CO_2:

$$\text{Feedstock}_{\text{CDR potential.}} = \frac{1000}{100} \cdot \beta \cdot M_{W,CO_2} \cdot \left(\frac{CaO}{M_{W,CaO}} + \frac{MgO}{M_{W,MgO}} + \frac{Na_2O}{M_{W,Na_2O}} + \frac{K_2O}{M_{W,K_2O}} - \frac{SO_4}{M_{W,SO_4}} - \frac{P_2O_5}{M_{W,P_2O_5}} \right) \quad (4)$$

Where:

1000/100 is a unit conversion that adjusts oxide weight percentages to kilograms per ton of feedstock;

β is the molar ratio of CO_2 storage potential to divalent alkalinity released from feedstock here 0.72[9]; and

$M_{w,\ldots}$ is the molar mass of the specific oxide computed from the constituent atomic masses (Table S3). Oxide abundances were taken as the mean of the XRF and ICP-OES determinations, except SO_4, which was calculated from the elemental S concentration measured by ICP-OES (Table S4).

We quantify Gross CDR through change in alkalinity export at the river mouth (KL) between the project and counterfactual scenarios (Equation 5), using an inverse-modelling approach to estimate CDR at the river mouth, thus integrating all gains and losses upstream:

$$\text{Gross CDR} = M\,(\eta_{Ocean} \cdot \text{Alk}_{\text{Export, Trial}} - C_{\text{Feedstock,Trial}}) \quad (5)$$

Where:

Gross CDR is in t CO_2e for the trial period

M converts moles C to t CO_2e

η_{Ocean} (unitless) is the ocean retention efficiency defined as change in oceanic DIC for a given change in alkalinity: $\Delta DIC_{ocean}/\Delta Alk_{ocean}$ in mol C eq^{-1} (calculated using sea surface temperature, salinity, and pCO_2).[9,47] During the period covered by the data η_{ocean} ranged from 0.81 to 0.91 with a mean of 0.86 (Figure S3; SI).

$\text{Alk}_{\text{Export, Trial}}$ (in eq) is the additional alkalinity exported from the river system by the trial, expressed as a difference between the total and counterfactual alkalinity exports:

$$\text{Alk}_{\text{Export, Trial}} = \text{Alk}_{\text{Export, Total}} - \text{Alk}_{\text{Export, Counterfactual}} \quad (6)$$

Where (for total or counterfactual):

$$\text{Alk}_{\text{Export, ...}} = \sum_{t=1}^{T} [Alk]_t\, Q_t\, \Delta t_t \quad (7)$$

Where:

Δt is the daily timestep (the summation represents all T timesteps comprising the reporting period of 98 days).

$[Alk]_t$ is the average alkalinity concentration in eq L^{-1} at daily timestep t;

Q_t is the average river flow in L s^{-1} at daily timestep t;

$Alk_{Export,Total}$ is the total alkalinity export at the river mouth (KL) during the trial, and was estimated by multiplying total alkalinity concentrations determined from bottle samples with the contemporaneous river discharge, averaged over the daily time step (t).

$Alk_{Export,Counterfactual}$ is the alkalinity export at the river mouth (KL) that would have occurred in the absence of additional liming associated with the trial; it is estimated using a linear regression predicting alkalinity at KL from alkalinity at the limed control tributary (LA), fit to 51 paired historical observations (Figure S1), then applied to the control-site alkalinity measured during the trial.

$C_{Feedstock,Trial}$ (moles C) for the trial period represents the additional calcite feedstock added to the river, and is expressed as:

$$C_{Feedstock,\ Trial} = C_{Feedstock,\ Total} - C_{Feedstock,\ Counterfactual} \quad (8)$$

Where $C_{Feedstock,Total}$ is the amount of calcite feedstock added at the Nyland doser during the trial expressed as:

$$C_{Feedstock\ Total} = \alpha \sum_{t=1}^{T} F_t \quad (9)$$

Where:

F_t is the mass of calcite feedstock (kg) dosed at daily timestep t, estimated from the slurry delivery volume and pump speed,

α is the conversion factor from mass of calcite feedstock to moles of C (mol kg^{-1}), derived from the carbon mass fraction in the calcite slurry, determined by combustion-based inorganic carbon analysis (Table S6).

$C_{Feedstock,\ Counterfactual}$ is the *business-as-usual* dosing rate amount; it was estimated from historical data using a multilevel linear model. The model was fitted using a subset of hourly calcite dose rates and river discharge data recorded at site NY (Jan 2023 and Feb – Dec 2024). This period was used to both minimize changes in dosing volume over time and to create a simulated continuous year of calcite addition data (avoiding gaps related to doser malfunctions). Since feedstock calcite is composed of fossil carbon, $C_{Feedstock,\ Trial}$ is subtracted from the DIC export for the project ($\eta_{Ocean} \cdot Alk_{Export,Trial}$), as the feedstock carbon does not represent the conversion of dissolved CO_2 to bicarbonate and therefore does not constitute additional CDR.

We estimate Net CDR as the Gross CDR minus project lifecycle greenhouse-gas emissions and the CDR that would have resulted from counterfactual weathering of the calcite feedstock:

$$\text{Net CDR} = \text{Gross CDR} - \text{Lifecycle Emissions} - \text{Counterfactual Weathering} \quad (10)$$

Where:

Lifecycle emissions are the total greenhouse gas emissions associated with the project, including those from operations, calcite extraction and transport (by boat between

Molde–Stavanger; 480 km), and via road from Stavanger–Nyland (152 km), quantified following ISO LCA standards (Table S7).

Counterfactual weathering refers to weathering of the calcite feedstock that would have occurred had the material not been used in the trial. Because this weathering would have occurred in the absence of the project, it is considered non-additional and is deducted from net CDR. Further details of the counterfactual-weathering calculation are provided in the Supporting Information.

Gross and Net CDR efficiencies are defined as Gross and Net CDR per tonne of calcite dosed (t CO_2e / t $CaCO_3$). Realized Gross and Net CDR are defined as fractions of Potential CDR (Equation 4). Realized Gross CDR therefore indicates the extent to which the observed field response approached the stoichiometric maximum, whereas Realized Net CDR additionally incorporates lifecycle-emissions and counterfactual-weathering deductions. Counterfactual Gross CDR derives directly from feedstock mass and the fixed conversion factor, thus its Gross CDR efficiency and realization reflect accounting assumptions rather than independently observed field performance.

The uncertainty for Gross CDR was estimated using a Monte Carlo simulation propagating distributions for discharge, measured alkalinity, predicted baseline alkalinity, calcite mass, calcite C fraction, and ocean retention factor ($\eta = 0.86 \pm 0.02$).

RESULTS & DISCUSSION

Impacts on Water Chemistry

During the trial, the increased calcite addition rate at the Nyland doser significantly altered chemistry at the limed downstream sites (OB and KL) relative to the unlimed upstream site (NY) and produced significant changes in river-mouth chemistry at KL relative to its historical baseline under conventional liming (Figure 2b). Immediately downstream of the doser (OB), mean pH increased significantly ($p < 0.001$) from 5.45 ± 0.25 at the upstream reference (NY) to 7.20 ± 0.14, accompanied by significant increases in total alkalinity (TA; 0.05 ± 0.01 to 0.21 ± 0.03 mmol L^{-1}), calcium (0.61 ± 0.07 to 4.31 ± 0.76 mg L^{-1}), ANC (29.5 ± 7.31 to 217 ± 44.3 µeq L^{-1}), conductivity (2.10 ± 0.36 to 3.67 ± 0.44 mS m^{-1}), and by a less significant increase in DIC (0.96 to 2.27 mg C L^{-1}; $p < 0.01$) (Table S8). At the river mouth (KL), the same carbonate variables were significantly elevated relative historic baseline (all $p < 0.001$; Table 1, Figure S5): pH rose from 6.24 to 6.86, TA, Ca^{2+} and ANC approximately doubled (0.067 to 0.151 mmol $L^{-1}$and 1.21 to 3.12 mg L^{-1}, and 64.2 to 154 µeq L^{-1}respectively) (Table 1).

Table 1. River-mouth water chemistry at KL: comparison of historical conditions (2011–2024) and the trial period

Parameter	Units	Historic Baseline [a]		Trial Period		Welch p	Significance
		Mean	SD	Mean	SD		
pH	unitless	6.24	1.74×10^{-1}	6.86	1.47×10^{-1}	8.42×10^{-14}	Significant
Total Alkalinity (TA) [b]	mmol L^{-1}	6.72×10^{-2}	1.06×10^{-2}	1.51×10^{-1}	2.48×10^{-2}	6.77×10^{-10}	Significant
Calcite saturation ($\log_{10}$ IAP/K_{sp})	Unitless	−4.45	2.04×10^{-1}	−2.97	2.44×10^{-1}	5.07×10^{-17}	Significant
Acid Neutralizing Capacity (ANC)	µeq L^{-1}	64.2	17.5	154	23.2	1.77×10^{-11}	Significant
Aluminum (reactive) [c]	mg L^{-1}	7.53×10^{-2}	2.97×10^{-2}	3.52×10^{-2}	1.46×10^{-2}	8.11×10^{-4}	Significant
Calcium	mg L^{-1}	1.21	2.29×10^{-1}	3.12	4.57×10^{-1}	3.49×10^{-11}	Significant
Magnesium	mg L^{-1}	3.01×10^{-1}	4.03×10^{-2}	4.17×10^{-1}	3.56×10^{-2}	5.47×10^{-11}	Significant

Parameter	Units	Historic Baseline [a]		Trial Period		Welch p	Significance
		Mean	SD	Mean	SD		
Sodium	mg L^{-1}	2.08	3.33×10^{-1}	2.88	2.88×10^{-1}	1.12×10^{-9}	Significant
Chloride	mg L^{-1}	3.05	5.81×10^{-1}	5.00	6.40×10^{-1}	5.11×10^{-10}	Significant
Conductivity	mS m^{-1}	2.10	2.48×10^{-1}	3.61	2.99×10^{-1}	7.59×10^{-14}	Significant
Potassium	mg L^{-1}	2.44×10^{-1}	4.74×10^{-2}	2.41×10^{-1}	2.43×10^{-2}	7.20×10^{-1}	Not significant
Sulphate (SO_4)	mg L^{-1}	1.20	2.29×10^{-1}	1.07	1.02×10^{-1}	5.48×10^{-3}	Significant [e]
Nitrate (NO_3-N)	mg L^{-1}	9.91×10^{-2}	2.88×10^{-2}	5.44×10^{-2}	2.40×10^{-2}	2.91×10^{-6}	Significant
Total phosphorus	mg L^{-1}	8.79×10^{-3}	4.45×10^{-3}	9.52×10^{-3}	3.91×10^{-3}	5.48×10^{-1}	Not significant
Total organic carbon (TOC)	mg L^{-1}	6.59	2.07	5.64	1.82	1.01×10^{-1}	Not significant

[a] Historical datasets were acquired from the national water database Vannmiljø (administered by the Norwegian Environment Agency). Values are total unless otherwise indicated. The historical baseline for station KL is the mean of NIVA's 2011–2024 monitoring data, trimmed to 10 June–15 September.

[b] Trial alkalinity is filtered, whereas the historical record is unfiltered.

[c] Trial sampling collected only filtered and unfiltered ICP-MS aluminum, while historic aluminum was analyzed as fractionated reactive Al. To account for the difference in sampling methodologies, the historical baseline is compared with the NIVA *business-as-usual* monthly sampling for the trial (n = 5).

We used PHREEQC to predict dissolution rate and calcite saturation. Kinetic modelling projected that approximately 95 % of the added calcite would dissolve within one hour (Figure S2a). At representative flow velocities of 0.5–1.0 m s^{-1}, this dissolution time corresponds to an estimated 95 % dissolution distance of 1.8–3.6 km; the OB station, therefore, lies well within the estimated dissolution zone, with only limited residual dissolution expected farther downstream. A sensitivity analysis varying the calcite saturation-state inhibition exponent γ (0.5–1) and the specific $CaCO_3$ surface area (1×10^6–5×10^6 cm^2 mol^{-1}) produced equilibrium pH values of 6.7–7.0, consistent with the observed median pH of 6.86 at KL (Figure S2b). The calculated calcite saturation ($\log_{10}$ IAP/K_{sp}) increased significantly downstream (from −4.45 at KL to −2.97 at OB), but the river nonetheless remained undersaturated with respect to calcite ($\Omega < 1$) throughout the trial, suggesting a low risk of secondary calcite precipitation.

The carbonate response was greatest at OB and attenuated toward KL, consistent with dilution during transport, including inflow from the Litleåne tributary (LA). Between OB and KL, mean TA decreased from 0.21 to 0.15 mmol L^{-1}, Ca^{2+} from 4.31 to 3.12 mg L^{-1}, ANC from 217 to 154 µeq $L^{-1}$and pH from 7.20 to 6.86. LA carried lower mean pH, TA, Ca^{2+} and ANC than OB (6.45, 0.09 mmol L^{-1}, 1.87 mg $L^{-1}$and 84.5 µeq L^{-1}, respectively), consistent with its calcite addition remaining unchanged at levels comparable to ordinary liming. Comparing the shifts in weathering signal, NY plots near the origin and close to the strong-acid (2:1) weathering line, whereas the downstream limed control, LA, extends along the 2:1 line, consistent with increased alkalinity generation but a minimal increase in DIC (Figure 2a). Under the increased calcite addition, OB shifts markedly toward the 1:1 line, suggesting a substantial increase in carbonic-acid weathering and alkalinity export. After mixing with LA, KL shifts back toward the 2:1 line but still exhibits substantially greater carbonic-acid weathering than upstream and ordinary liming conditions (Figure 2a).

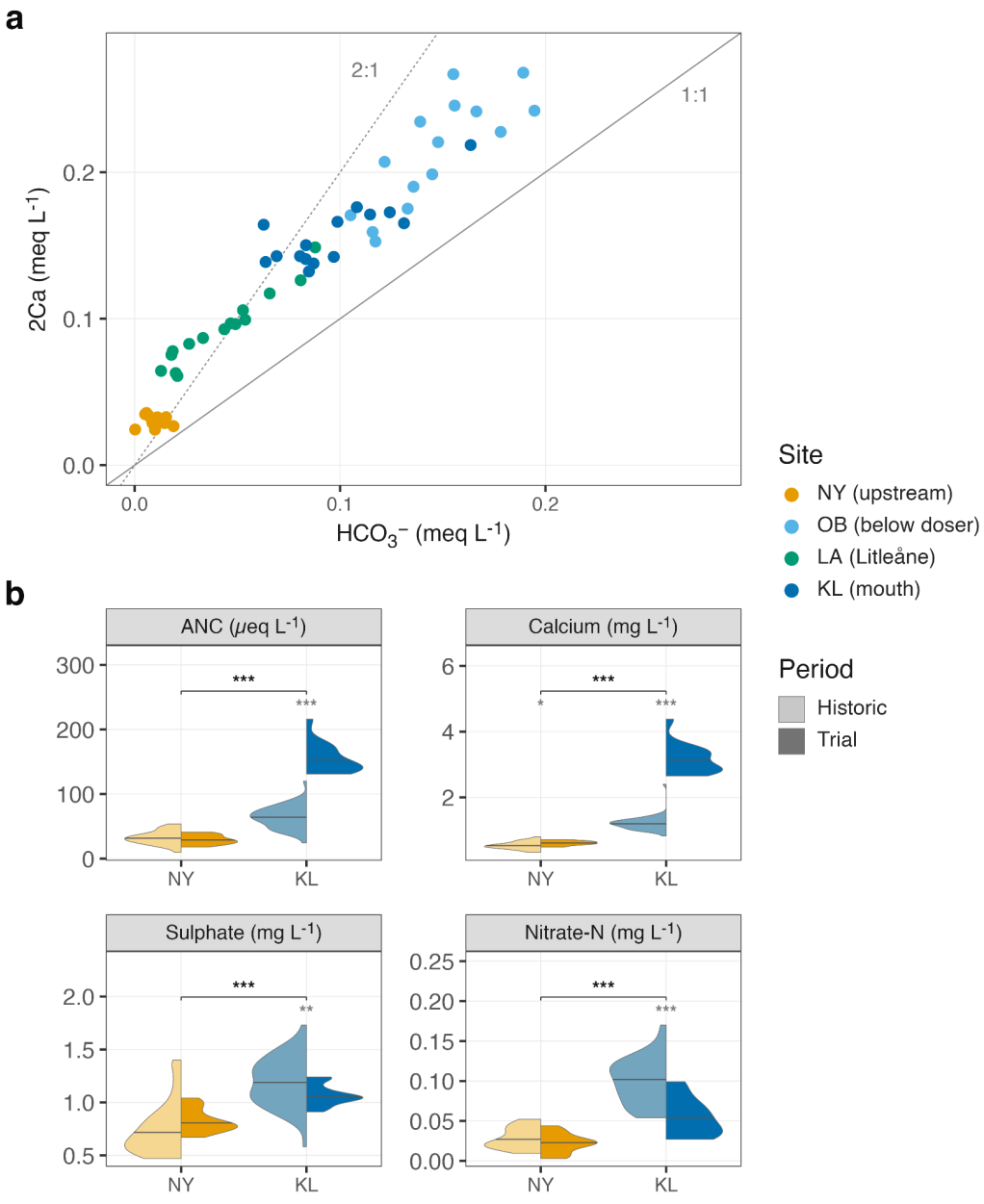

Figure 2. Carbonate-weathering signature and historical-versus-trial water chemistry during the Kvina trial. **(a)** Relationship between charge-equivalent calcium, $2Ca^{2+}$, and HCO_3^-, for samples collected at the upstream station (NY), weathering zone (OB), limed control tributary (LA), and the river mouth (KL). HCO_3^- was calculated as carbonate alkalinity by correcting measured total alkalinity for organic-acid contributions using a triprotic model parameterized with each

sample's DOC, pH, and alkalinity.[48] Solid 1:1 and dashed 2:1 lines represent carbonate weathering by carbonic and strong acids, respectively. **(b)** Split-violin distributions of ANC, calcium, sulphate, and nitrate at NY and KL for the season-matched historical baseline and trial. Two-sided Welch's t-tests where * $p < 0.05$, ** $p < 0.01$, *** $p < 0.001$. Grey stars denote trial-versus-historical differences within stations; black brackets and bold stars denote trial-period NY–KL differences. Filtered values are used.

During the trial at the river mouth (KL), major ions (Na^+, Mg^{2+} and Cl^-) were higher than the historic baseline (2.88 vs 2.08, 0.417 vs 0.301 and 5.00 vs 3.05 mg L^{-1}, respectively; all $p < 0.001$; Table 1), yet during the trial none changed significantly from NY to OB (Table S8). Elevated concentrations at NY, KL, and LA relative to the historical baseline across the full 2025 record suggest these increases were not attributable to the trial (Figure S4, SI).

Most nutrients showed no significant differences from upstream to downstream throughout the trial (NY vs OB; Table S8). Mean TOC and DOC were statistically unchanged (TOC 5.82 and 5.94 mg L^{-1}; DOC 5.69 and 5.83 mg C L^{-1}), as were nitrate (0.020 and 0.027 mg N L^{-1}), total phosphorus (7.7 and 8.2 µg L^{-1}) and sulphate (0.83 and 0.83 mg L^{-1}) (Figure S9). One exception was phosphate (PO_4-P; 1.07 to 1.93 µg P L^{-1}; $p < 0.001$). Some of the increase in phosphate between OB and KL may be consistent with trace masses present in the feedstock (Table S4). However, consistent increases in nitrate and total phosphorus at downstream sites relative to upstream sites are consistent with agricultural inputs (Figure S10). During the trial, sulphate and nitrate concentrations at the river mouth differed significantly from the historical baseline (Table 1); however, neither differed between NY and OB (Table S8). Together with the absence of

significant changes in TOC and total phosphorus, this suggests that the treatment did not alter the organic-carbon or nutrient regime (SI).

Figure 3. Weekly grab sample values for turbidity, dissolved aluminum and dissolved iron upstream of the Nyland doser (NY) and downstream (OB), with mean daily river discharge (at KL) for the trial period.

No trace metals increased significantly between NY and OB during the trial, including Al, As, Cd, Cr, Cu, Fe, Ni, Pb, U, V, and Zn (Figure 3; Table S8). There were significant decreases for

filtered manganese (8.52 to 3.77 µg L^{-1}; $p < 0.001$) and cobalt (0.095 to 0.068 µg L^{-1}; $p < 0.05$). Reactive aluminum was measured only in water samples from NY and KL and decreased significantly downstream during the trial window (0.067 to 0.035 mg L^{-1}; $p < 0.05$). The significant downstream decreases in filtered Mn, Co and reactive Al suggest precipitation or partitioning mechanisms (e.g., Al-rich oxyhydroxide flocs scavenging Mn through sorption or coprecipitation).

Turbidity did not increase significantly below the doser (NY vs OB; Figure 3) and remained low at KL (0.37–1.50 FNU; mean 0.74 FNU), which is below the levels at which suspended sediment begins to affect salmonid behaviour (~5 FTU).[49,50] Mean daily discharge at KL during the trial was 35.8 m^3 s^{-1} (ranging from 9.48 to 333 m^3 s^{-1}). Two rainfall events increased river discharge in August and September (Figure 3); during these episodes, higher velocities are suspected to have extended the dissolution zone, causing a brief increase in turbidity (Figure 3).

CDR Quantification and Efficiency

During the trial, 1 749 ± 8 t of calcite slurry (744 ± 4 t CO_2e) were added at the Nyland doser: 1 480 ± 9 tonnes (629 ± 5 CO_2e) for the trial (additional), and 269 ± 4 tonnes (114 ± 2 CO_2e) for the counterfactual scenario (Table 2). Relative to the same period, the mean project addition rate exceeded the historical dosing rate by approximately 140 %, raising the continuous sensor pH downstream of the weathering zone at KV by 0.7 pH units (Figure 4). The counterfactual alkalinity-export model predicted alkalinity to within a root-mean-square error (RMSE) of 0.011 mmol L^{-1} and pH with an RMSE of 0.12 units (Figure S1).

Table 2. Gross, Net and Counterfactual CDR Calculations for the trial period

Condition	**Trial Scenario** (Additional, calcite needed to raise pH target from 6.0 to 7.0)	**Counterfactual Scenario** (Non-Additional, calcite needed to raise pH target from background to 6.0)	**Upstream Unlimed** Control station (NY)	**Total impact** (trial + counterfactual; all dosing activities)
$C_{feedstock}$ (t CO_2e) added	629 ± 5	114 ± 2	0	744 ± 4
Dry weight calcite feedstock dosed (t dry product)	1 480 ± 9	269 ± 4	0	1 749 ± 8
Q (m^3/s) at river mouth (KL) average daily, (range)	35.8 (9.48 - 333)			
η_{ocean} (set value over study period)	0.86 ± 0.02			
Alkalinity Export (t CO_2e)	1020 ± 40	229 ± 4	660 ± 30	1 910 ± 20
Gross CDR (t CO_2e)	250 ± 30	83 ± 1	0	330 ± 30
LCA Emissions (t CO_2e)	35.9 [f]	6.52 [g]	0	42.4
Counterfactual weathering of calcite feedstock (t CO_2e)	100.1 [f]	18.2	0	118.3
Net CO_2e removed (t CO_2e) (total ± 1 σ)	110 ± 30	58 ± 1	0	170 ± 30
Gross efficiency ratio (t CO_2e / t feedstock)	0.17 ± 0.02	0.307 [h]	–	0.19 ± 0.02
Net efficiency ratio (t CO_2e / t feedstock)	0.07 ± 0.02	0.215 ± 0.001	–	0.10 ± 0.02

[f] Conservative values are used to define an upper limit rather than using standard deviation.

[g] Estimated using ($C_{feedstock,\ Counterfactual}$ / $C_{feedstock,\ Treatment}$)·Operating Emissions; where ($C_{feedstock,\ Counterfactual}$ / $C_{feedstock,\ Treatment}$) is the ratio of calcite feedstock dosed under the two scenarios, and where Operating Emissions represent emissions from additional operating activities as calculated in the LCA.

[h] Assumed based on calcite feedstock properties (factor of 0.307 t CO2e per t calcite feedstock); standard deviation is therefore zero, since CDR for the counterfactual scenario is estimated from the feedstock dose alone.

Total measured alkalinity export at KL was 1 910 ± 20 t CO_2e, comprised of 660 ± 30 t CO_2e of natural baseline export, 229 ± 4 t CO_2e attributable to the counterfactual dose and 1 020 ± 40 t CO_2e attributable to the additional trial dose (Table 2, Figure 5d). After deducting feedstock carbon and ocean uptake efficiency losses, the total combined Gross CDR from the trial and counterfactual scenarios was 330 ± 30 t CO_2e. Of this total, 250 ± 30 t CO_2e was considered

additional as a result of the trial (Figure 5b, c), while 83 ± 1 t CO_2e was attributable to the counterfactual scenario as a result of *business as usual* liming (Table 2).

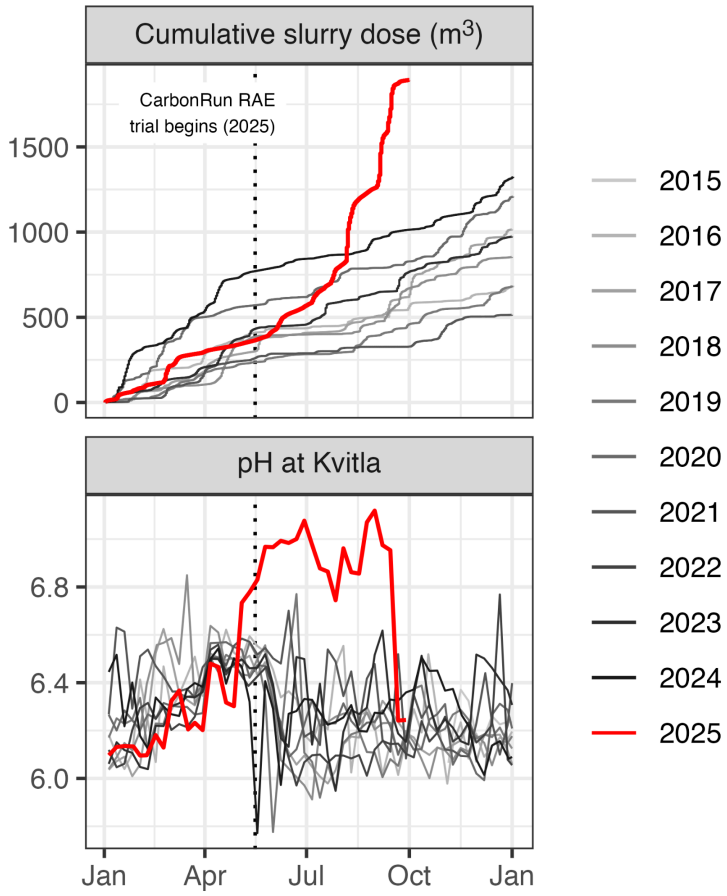

Figure 4. Slurry dose and pH during Kvina Trial and for earlier years (2015-2024). Top: Cumulative daily slurry dose at Nyland doser; Bottom: mean daily pH at Kvitla (KV), downstream of the Nyland doser. Slurry dosing data collected in 2015 and 2022 were omitted due to errors.

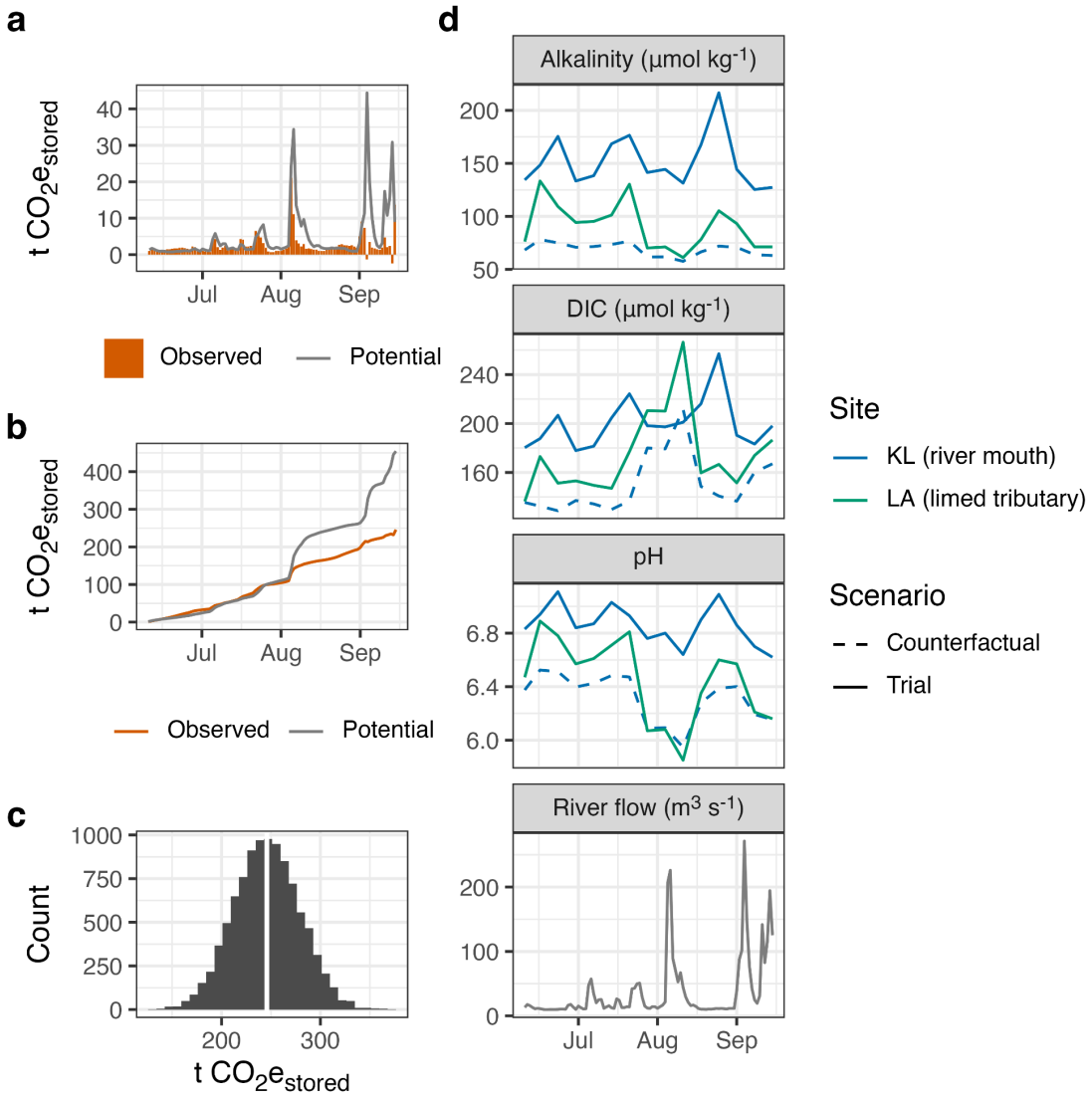

Figure 5. Carbonate chemistry, discharge and CDR estimates during the trial. **(a)** Project and potential Gross CDR calculated on a daily timestep, where potential CDR is estimated using a conversion factor of 0.307 t CO_2e per t calcite feedstock, with the $\eta_{ocean} = 0.86$ accounting for the conversion of alkalinity to oceanic CO_2 storage and associated losses from DIC re-equilibration. **(b)** Cumulative Project vs. potential CDR calculated on a daily timestep. **(c)** Monte Carlo prediction of cumulative gross CDR **(d)** Carbonate system variables (Alkalinity, DIC and pH) for the project and counterfactual scenarios during the trial. Time series of total alkalinity, DIC

(calculated from weekly pH, alkalinity, and in-situ temperature samples), and river flow (recorded hourly, aggregated here to daily).

Total alkalinity measured export at KL was 1 910 ± 20 t CO_2e, comprised of 660 ± 30 t CO_2e of natural baseline export, 229 ± 4 t CO_2e attributable to the counterfactual dose and 1 020 ± 40 t CO_2e attributable to the additional trial dose (Equation 6, Table 2, Figure 5c). After deducting feedstock carbon and ocean uptake efficiency losses, the total combined Gross CDR from the trial and counterfactual scenarios was 330 ± 30 t CO_2e. Of this total, 250 ± 30 t CO_2e was considered additional as a result of the trial (Figure 5b, c), while 83 ± 1 t CO_2e was attributed to the counterfactual scenario as a result of *business as usual* liming (Table 2).

The calcite feedstock added under the project scenario had a Feedstock $_{\text{CDR potential}}$ of 0.307 t CO_2e / t feedstock (Equation 4), corresponding to a Potential CDR of 454 t CO_2e for the trial. The realized Gross CDR corresponded to 54 % of the stoichiometric maximum, or 0.17 ± 0.02 t CO_2e per t feedstock, after propagating uncertainty using a Monte Carlo simulation (the resulting distribution is shown in Figure 5c).

Realized gross CDR closely tracked potential CDR from 10 June until the 4 August discharge event, with a cumulative realized-to-potential ratio of 94 % (Figure 5a, b). Following the flow peak, this ratio declined to 69 % by 13 August, indicating that realized gross CDR was approximately 27–32 % below its potential during the runoff episode; comparable shortfalls recurred during most subsequent high-flow events (Figure 5a, b). Gross CDR approached its potential most closely under higher-pH, lower-discharge conditions. Raising river pH from approximately 5.4 to 6 required 269 t of calcite, whereas reaching pH 7 required an additional 1 480 t, for a total of 1 749 t, 6.5 times the amount required to reach pH 6. This nonlinear

increase is consistent with H_2CO_3/HCO_3^- buffering near pH 6.3, where added carbonate primarily increases bicarbonate alkalinity rather than pH.

Gross CDR realization may be reduced by several factors: incomplete or delayed alkalinity export, transport losses, or transformation (including conversion to organic alkalinity decreasing measured inorganic alkalinity), and limited sampling resolution during high flow. Our results show that the realized Gross CDR decreased with increasing discharge. We hypothesize that a key contributor to the lowered efficiency during high runoff episodes is the low temporal resolution of grab samples used to produce the alkalinity export model: monthly for historical sampling, and weekly during the trial. These discretizations result in poorly resolved alkalinity concentrations relative to the potential discharge variance at the corresponding timesteps. Because feedstock fossil-carbon is continuously measured directly at the doser, this approach reduces the resolution of the alkalinity-export signal relative to the fossil-carbon deduction, lowering apparent CDR efficiency without materially changing the underlying reaction pathways.

The ratio of realized Gross CDR (Equation 5) to potential CDR (Equation 4) also increases, up to a point, with final pH after dosing; this is mainly due to buffering by organic acids. That is, at lower final pH, a larger share of the added alkalinity neutralizes organic acids and is expressed as organic anions; because this pathway is excluded from our Gross CDR calculation, that fraction is not credited. Further, the historical dataset and thus the baseline model do not capture acid episodes very well, again due to the weekly/monthly frequency of grab sample data collection.

Thus, to increase alkalinity recovery at the river mouth and reduce uncertainty for Gross CDR, we recommend: 1) Collecting a station-specific pre-trial baseline to reduce reliance on historical

grab-sample records, and train and validate the counterfactual model under contemporary hydrological and chemical conditions; 2) Increase temporal resolution during baselining and the trial via more frequent grab sampling and/or improved reliance continuous in situ sensor measurements to strengthen the predictive relationship between limed control tributary (LA) and the river mouth (KL); 3) Install a discharge gauge at the river mouth to avoid reliance on extrapolation of discharge from an upstream gauge, thus directly constraining the alkalinity flux calculation that underpins both Gross CDR and the counterfactual baseline. Combined, these improvements are likely to substantially reduce the uncertainty for Gross CDR and improve the agreement between added alkalinity and downstream measurements.

Trial lifecycle emissions totalled 35.9 t CO_2e (14.6 % of Gross CDR), dominated by feedstock sourcing, processing and transport (Table S7); counterfactual calcite feedstock weathering accounted for a further 100.1 t CO_2e (equivalent to 40.7 % of Gross CDR). After deducting these emissions from Gross CDR, the trial yielded a Net CDR of 110 ± 30 t CO_2e (Table 2). Disregarding additionality, combined Net CDR was 170 ± 30 t CO_2e (110 ± 30 trial and 58 ± 1 counterfactual). Net CDR efficiencies were 0.07 ± 0.02 and 0.215 ± 0.001 t CO_2e (t $CaCO_3$)$^{-1}$ for the project and counterfactual. Gross and Net CDR efficiencies for the combined counterfactual and trial liming were 0.19 ± 0.02 and 0.10 ± 0.02 t CO_2e (t $CaCO_3$)$^{-1}$, respectively.

Annual Gross CDR was projected by scaling the 98-day CDR-to-discharge relationship to annualized discharge volume; using mean annual discharge from 2015–2024 (excluding years with incomplete records) yields an estimated Gross CDR of 1 140 t CO_2e yr $^{-1}$.

Mechanistic Interpretation of RAE Weathering Reactions

A conceptual framework for the Kvina trial, together with idealized limed and unlimed catchments, illustrates how RAE can generate CDR across weathering pathways (carbonic, strong, or organic acid-dominated) (Figure 6). Under the current CDR quantification, the relevant metric is not whether carbonate-derived DIC export increases, but if alkalinity delivery to the ocean increases. An increase in ocean alkalinity relative to the counterfactual scenario represents an increase in the ocean's capacity to store carbon[51] even when riverine DIC is not increased directly.

In the acidic unlimed catchment with low pH (~5.6; Figure 6a), any exported riverine acidity (strong, organic or carbonic) results in the downstream release of CO_2. In a catchment dominated by strong mineral or organic acids, the consumption of marine alkalinity during oceanic equilibration constitutes a negative alkalinity export and reduces the ocean's capacity to store carbon. In an equivalent carbonic acid-dominated system the majority of DIC existss as CO_2 driving CO_2 evasion within the river and during ocean equilibration. If alkalinity is added to the catchment to raise pH (~7.0; Figure 6b), it is consumed by acids (strong, carbonic or organic) in some combination. When neutralization occurs with carbonic acid, the resulting shift in DIC speciation toward bicarbonate promotes the retention of riverine DIC and increases alkalinity export to the ocean, which constitutes CDR relative to the counterfactual offgassing of DIC during oceanic re-equilibration. Equivalently, neutralization of exported strong-mineral acids – and potentially weak organic acids – that would otherwise consume marine alkalinity, and reduce

the capacity of receiving waters to absorb and retain atmospheric CO_2, can also be considered CDR despite the release of CO_2 during neutralization.

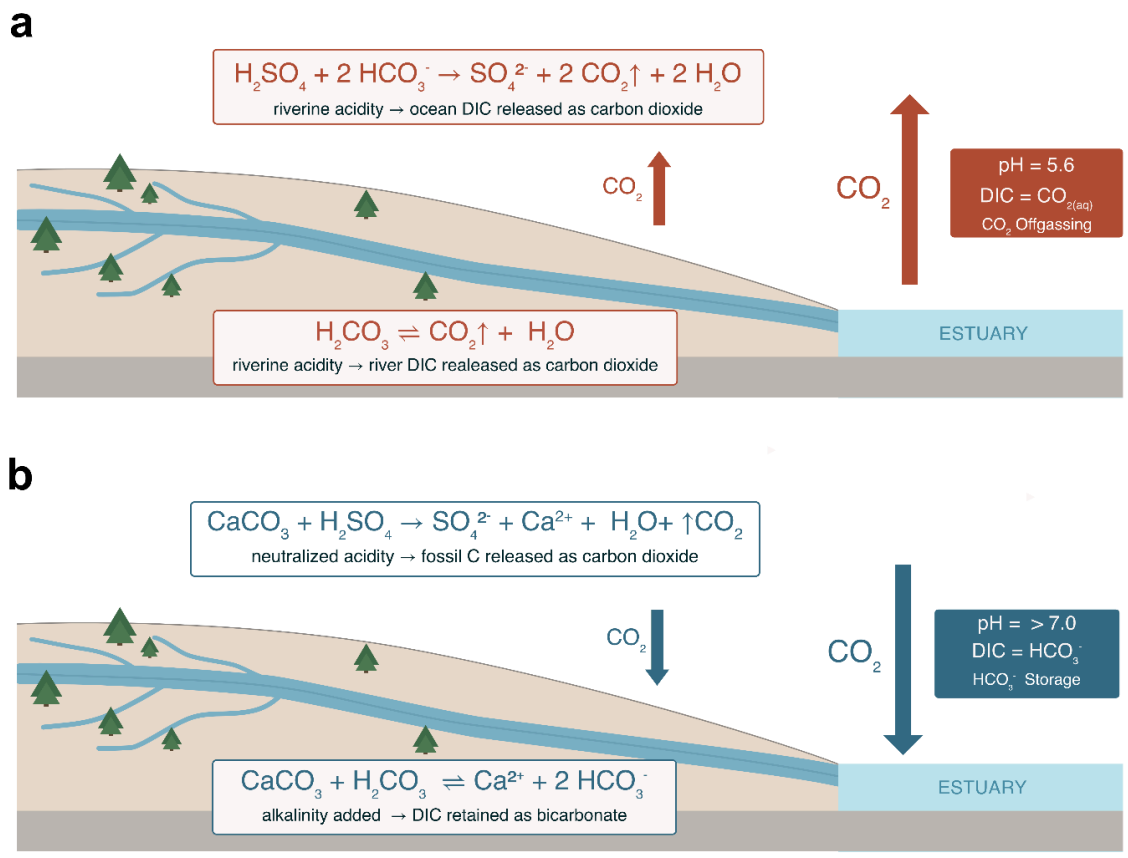

Figure 6. Conceptual comparison of carbon cycling and CDR in limed and unlimed rivers **(a)** Unlimed catchment where acid neutralization consumes bicarbonate alkalinity and degassing releases riverine DIC as CO_2; **(b)** Limed catchment (equivalent to the Kvina trial) where $CaCO_3$ addition neutralizes acidity and/or converts CO_2/carbonic acid into Ca^{2+} and HCO_3^-, increasing alkalinity export and ocean CO_2 retention. Sulfuric acid is shown as a representative acid but could be replaced by other strong mineral or organic acids.

Within this framework, calcite addition during the Kvina trial raised the pH target and shifted the carbonate system toward bicarbonate dominance (Figure 6b). Under the lower-pH counterfactual liming, calcite-derived DIC would instead have likely been reprotonated and released as CO_2 through gas evasion (Figure 2a; Equation 2). The limited contemporary input of strong acids, together with the coupled increases in carbonate alkalinity and Ca^{2+} observed under increased dosing during the trial (Figure 2a), suggests that most additional calcite dissolution occurred via the carbonic-acid pathway, thereby increasing both alkalinity and DIC export.

Implications for RAE Deployments

Our results suggest that CDR can be quantified and delivered by increasing pH targets within existing river-liming programs, positioning rivers as a promising deployment pathway along the LOAC. RAE benefits from the presence of existing infrastructure, permitting pathways, stakeholder and community relations, multi-decadal ecologic, water chemistry data sets and calcite feedstock supply chains, all of which can reduce deployment time and costs, common challenges for CDR projects. RAE nevertheless faces several deployment constraints. Existing river-liming programs are concentrated in relatively small, naturally acidified catchments, which may limit the volume of alkalinity that can be added and therefore the achievable scale of CDR. Furthermore, the often-remote locations can also increase feedstock transport requirements, costs, and associated life-cycle emissions. In larger rivers, the limestone quantities required to produce a detectable CDR signal, together with the potential for incomplete feedstock dissolution, may further complicate dosing control and increase quantification uncertainty.

An important distinction should be made between the Water Framework Directive (WFD; Directive 2000/60/EC) ecological targets and general water quality targets. Under WFD,

ecological status is assessed relative to historical reference conditions based on water chemistry before significant human influence, rather than to ecological optima.[52] The limed lower Kvina has contemporary water chemistry consistent with the Norwegian lowland, lime-poor, clear-water river type, characterized by calcium concentrations of 1–4 mg L^{-1}, alkalinity of 0.05–0.2 meq L^{-1} and TOC of 2–5 mg L^{-1}.[53] Accordingly, although trial conditions may not have exceeded these thresholds, the increases in pH, calcium, and alkalinity likely moved the river beyond the typical ecological targets for naturally soft, humic waters.

Independent of WFD reference conditions, water chemistry remained within ranges considered protective of salmonids and most freshwater biota, and the observed changes were well below those associated with disrupted nutrient cycling, increased ammonia toxicity, or altered phytoplankton community composition (Table S9).[54–56] Ecotoxicological benchmarks, including a pH of approximately 6.5 for salmonid health and calcium thresholds derived from *Daphnia* studies, likewise indicate that trial conditions remained environmentally appropriate. The ecological case for CDR in Norwegian rivers is therefore nuanced. Where liming offsets anthropogenic acidification beyond natural variability, increasing pH can provide genuine ecological benefits, particularly for salmonids and aluminum-sensitive taxa. However, a type-specific management approach should be applied to minimize ecosystem stress and maintain conditions near a natural reference state. Because CDR can be achieved with only a modest increase in dosing, moderate increases in year-round pH targets at existing liming sites may enable CDR while balancing ecological objectives. Future deployments could also prioritize larger or less strongly acidic rivers, where greater CDR may be achievable without a proportional increase in ecological risk.

Limitations and Future Research

Several limitations constrain the application of the study results. Notably, most changes in water chemistry were derived from grab-sample measurements, as data-quality limitations and substantial data loss rendered most *in-situ* sensor records unsuitable for quantitative analysis. Further, the three-month summer trial in the Kvina River does not capture seasonal or interannual variability; thus the transferability of trial results to other catchments will depend on differences in water chemistry, land use, hydrological regime, and biogeochemical processing. Relative to OAE, RAE also exhibits greater spatial heterogeneity between deployment environments; consequently, results from individual river systems should be extrapolated with caution. Additionally, further study of long-term ecosystem responses to prolonged elevations in alkalinity, pH, and Ca^{2+} is needed to better characterize potential ecologic impacts associated with increased liming.

Recommendations for future studies are to better constrain in-river alkalinity loss pathways, including riverine photosynthesis, respiration driven decomposition[57], and rapid pH shifts inducing CO_2 outgassing.[58] Estuarine processes also require further investigation, particularly continued organic-acid deprotonation during river–seawater mixing and its implications for alkalinity retention. Quantifying these processes across relevant spatial and temporal scales will be necessary for RAE to scale as a CDR pathway and to evaluate assumptions that underpin current ERW and OAE quantification frameworks.

CONFLICT OF INTEREST DISCLOSURE

Miljødirektoratet, the Kommune of Kvinesdal, and Omya conceived the original idea for the Kvina Trial. Author S.M. Sterling is a co-founder and employee of CarbonRun CDR Ltd., which has a commercial interest in RAE CDR project development. As of July 30th, 2026, Authors I. Bahler, B. Trueman, C. Brenan and J. Tucker are employed by, and/or hold equity in, CarbonRun. Author R. Vogt declares no conflicts of interest.

ASSOCIATED CONTENT

The following files are Available free of charge,

- **Supporting Information (**docx**):**
    - Includes water-chemistry sampling and analytical protocols; calcite-dissolution kinetics; feedstock mineralogy, elemental and oxide composition, stoichiometric conversion factors; oceanic re-equilibration losses and retention factor methods; life-cycle emissions inventory; methods for calculation of counterfactual feedstock weathering; extended historical water chemistry data, cumulative Ca and Mg export across the Nyland dosing reach; and potential ecological responses to pH elevation during river alkalinity enhancement.

- **Scripts and Data (https://github.com/cr-bft/kvina-trail.git):**
    - Data and analysis code for the Kvina/Litleåne river-liming CDR study, including historical and trial water-chemistry data; station and analyte registries; R code for DOC-corrected alkalinity, calcite saturation, statistical comparisons, and all manuscript figures; discharge, dosing, and feedstock records; baseline-dose, PyCO2SYS, PHREEQC, and Monte Carlo models supporting the CDR estimate.

ACKNOWLEDGMENTS

We thank the Norwegian Environment Agency (*Miljødirektoratet*) for approving the trial and Kvinesdal Municipality for access to the Nyland lime doser and logistical support during the trial. We thank the Norwegian Institute for Water Research (NIVA), Liv Bente Skancke, Tina Bryntesen, and Øyvind Kaste for supporting access to historical water-chemistry data, and Al Magne Versland (Powafa), Alix Broughton, Patrick Duke, Tristan Davies and Eddie Halfyard for field, analysis and editorial support (CarbonRun). Jennifer Yin is thanked for her effort developing the Isometric River Alkalinity Enhancement (RAE) Protocol. Northwest Hydraulic Consultants (nhc) supported development of the hydrological model used to predict discharge at the river mouth. Miljødirektoratet funded routine dosing operations and historical monitoring. CarbonRun funded additional dosing, limestone and its delivery, river monitoring, grab-sample analysis, and data analysis, with support from Frontier through an offtake purchase of CDR credits. Author RDV's work is partly funded by a contribution from the Research Council of Norway (contract no. 342628/L10). Author SMS's work is partly funded by contributions from Norges Forskningsråd (Grant ID: 342628/L10); Canada First Research Excellence Fund (Grant ID: TCA-LRP-20241-2.1-04) and Natural Sciences and Engineering Research Council of Canada (Grant ID: RGPIN06958-19).

REFERENCES

(1) United Nations Environment Programme. *Emissions Gap Report 2025*; United Nations Environment Programme (UNEP), 2025. https://www.unep.org/resources/emissions-gap-report-2025.

(2) Mace, M. J.; Fyson, C. L.; Schaeffer, M.; Hare, W. L. Large‐Scale Carbon Dioxide Removal to Meet the 1.5°C Limit: Key Governance Gaps, Challenges and Priority Responses. *Glob. Policy* **2021**, *12* (S1), 67–81. https://doi.org/10.1111/1758-5899.12921.

(3) Buck, H. J.; Carton, W.; Lund, J. F.; Markusson, N. Why Residual Emissions Matter Right Now. *Nat. Clim. Change* **2023**, *13* (4), 351–358. https://doi.org/10.1038/s41558-022-01592-2.

(4) IPCC. *Climate Change 2023: Synthesis Report. Contribution of Working Groups I, II and III to the Sixth Assessment Report of the Intergovernmental Panel on Climate Change*; Lee, H., Romero, J., Eds.; 2023. https://doi.org/10.59327/IPCC/AR6-9789291691647.

(5) Edwards, M. R.; Geden, O.; Gidden, M. J.; Lamb, W. F. *The State of Carbon Dioxide Removal 2026 (3rd ed.)*. https://doi.org/10.17605/OSF.IO/ZRD65.

(6) Lieber, A.; Morrow, C.; Stabile, J.; Hornbostel, K. A Comparative Review of Terrestrial and Marine Carbon Dioxide Removal (CDR) Methods. *Carbon Capture Sci. Technol.* **2026**, *18*, 100550. https://doi.org/10.1016/j.ccst.2025.100550.

(7) Archer, D.; Kheshgi, H.; Maier‐Reimer, E. Multiple Timescales for Neutralization of Fossil Fuel CO_2. *Geophys. Res. Lett.* **1997**, *24* (4), 405–408. https://doi.org/10.1029/97GL00168.

(8) Kanzaki, Y.; Planavsky, N. J.; Reinhard, C. T. New Estimates of the Storage Permanence and Ocean Co-Benefits of Enhanced Rock Weathering. *PNAS Nexus* **2023**, *2* (4). https://doi.org/10.1093/pnasnexus/pgad059.

(9) Renforth, P.; Henderson, G. Assessing Ocean Alkalinity for Carbon Sequestration. *Rev. Geophys.* **2017**, *55* (3), 636–674. https://doi.org/10.1002/2016RG000533.

(10) Ridgwell, A.; Zeebe, R. The Role of the Global Carbonate Cycle in the Regulation and Evolution of the Earth System. *Earth Planet. Sci. Lett.* **2005**, *234* (3–4), 299–315. https://doi.org/10.1016/j.epsl.2005.03.006.

(11) Regnier, P.; Resplandy, L.; Najjar, R. G.; Ciais, P. The Land-to-Ocean Loops of the Global Carbon Cycle. *Nature* **2022**, *603* (7901), 401–410. https://doi.org/10.1038/s41586-021-04339-9.

(12) Beerling, D. J.; Kantzas, E. P.; Lomas, M. R.; Wade, P.; Eufrasio, R. M.; Renforth, P.; Sarkar, B.; Andrews, M. G.; James, R. H.; Pearce, C. R.; Mercure, J.-F.; Pollitt, H.; Holden, P. B.; Edwards, N. R.; Khanna, M.; Koh, L.; Quegan, S.; Pidgeon, N. F.; Janssens, I. A.;

Hansen, J.; Banwart, S. A. Potential for Large-Scale CO2 Removal via Enhanced Rock Weathering with Croplands. *Nature* **2020**, *583* (7815), 242–248. https://doi.org/10.1038/s41586-020-2448-9.

(13) Beerling, D. J.; Reinhard, C. T.; James, R. H.; Khan, A.; Pidgeon, N.; Planavsky, N. J. Challenges and Opportunities in Scaling Enhanced Weathering for Carbon Dioxide Removal. *Nat. Rev. Earth Environ.* **2025**, *6* (10), 672–686. https://doi.org/10.1038/s43017-025-00713-7.

(14) Hartmann, J.; West, A. J.; Renforth, P.; Köhler, P.; De La Rocha, C. L.; Wolf‐Gladrow, D. A.; Dürr, H. H.; Scheffran, J. Enhanced Chemical Weathering as a Geoengineering Strategy to Reduce Atmospheric Carbon Dioxide, Supply Nutrients, and Mitigate Ocean Acidification. *Rev. Geophys.* **2013**, *51* (2), 113–149. https://doi.org/10.1002/rog.20004.

(15) D'Ascanio, R.; Vanderkloot, E.; Vu, K.; Raymond, P. A.; Planavsky, N.; Katchinoff, J. A. Precise Monitoring of Enhanced Weathering in Wastewater Treatment Facilities via a Mass Balance Approach; 2024.

(16) Kitidis, V.; Rackley, S. A.; Burt, W. J.; Rau, G. H.; Fawcett, S.; Taylor, M.; Tarran, G.; Woodward, E. M. S.; Harris, C.; Fileman, T. Magnesium Hydroxide Addition Reduces Aqueous Carbon Dioxide in Wastewater Discharged to the Ocean. *Commun. Earth Environ.* **2024**, *5* (1). https://doi.org/10.1038/s43247-024-01506-4.

(17) Meybeck, M. Global Chemical Weathering of Surficial Rocks Estimated from River Dissolved Loads. *Am. J. Sci.* **1987**, *287* (5), 401–428. https://doi.org/10.2475/ajs.287.5.401.

(18) Raymond, P. A.; Hartmann, J.; Lauerwald, R.; Sobek, S.; McDonald, C.; Hoover, M.; Butman, D.; Striegl, R.; Mayorga, E.; Humborg, C.; Kortelainen, P.; Dürr, H.; Meybeck, M.; Ciais, P.; Guth, P. Global Carbon Dioxide Emissions from Inland Waters. *Nature* **2013**, *503* (7476), 355–359. https://doi.org/10.1038/nature12760.

(19) Liu, M.; Raymond, P. A.; Lauerwald, R.; Zhang, Q.; Trapp-Müller, G.; Davis, K. L.; Moosdorf, N.; Xiao, C.; Middelburg, J. J.; Bouwman, A. F.; Beusen, A. H. W.; Peng, C.; Lacroix, F.; Tian, H.; Wang, J.; Li, M.; Zhu, Q.; Cohen, S.; van Hoek, W. J.; Li, Y.; Li, Y.; Yao, Y.; Regnier, P. Global Riverine Land-to-Ocean Carbon Export Constrained by Observations and Multi-Model Assessment. *Nat. Geosci.* **2024**, *17* (9), 896–904. https://doi.org/10.1038/s41561-024-01524-z.

(20) Dean, J. F.; Coxon, G.; Zheng, Y.; Bishop, J.; Garnett, M. H.; Bastviken, D.; Galy, V.; Spencer, R. G. M.; Tank, S. E.; Tipper, E. T.; Vonk, J. E.; Wallin, M. B.; Zhang, L.; Evans, C. D.; Hilton, R. G. Old Carbon Routed from Land to the Atmosphere by Global River Systems. *Nature* **2025**, *642* (8066), 105–111. https://doi.org/10.1038/s41586-025-09023-w.

(21) Zhang, S.; Planavsky, N. J.; Katchinoff, J.; Raymond, P. A.; Kanzaki, Y.; Reershemius, T.; Reinhard, C. T. River Chemistry Constraints on the Carbon Capture Potential of Surficial

Enhanced Rock Weathering. *Limnol. Oceanogr.* **2022**, *67* (S2). https://doi.org/10.1002/lno.12244.

(22) Dreybrodt, W.; Lauckner, J.; Zaihua, L.; Svensson, U.; Buhmann, D. The Kinetics of the Reaction CO2 + H2O → H+ + HCO3− as One of the Rate Limiting Steps for the Dissolution of Calcite in the System H2O-CO2-CaCO3. *Geochim. Cosmochim. Acta* **1996**, *60* (18), 3375–3381. https://doi.org/10.1016/0016-7037(96)00181-0.

(23) Wallin, M.; Buffam, I.; Öquist, M.; Laudon, H.; Bishop, K. Temporal and Spatial Variability of Dissolved Inorganic Carbon in a Boreal Stream Network: Concentrations and Downstream Fluxes. *J. Geophys. Res. Biogeosciences* **2010**, *115* (G2), 2009JG001100. https://doi.org/10.1029/2009JG001100.

(24) Ulseth, A. J.; Hall, R. O.; Boix Canadell, M.; Madinger, H. L.; Niayifar, A.; Battin, T. J. Distinct Air–Water Gas Exchange Regimes in Low- and High-Energy Streams. *Nat. Geosci.* **2019**, *12* (4), 259–263. https://doi.org/10.1038/s41561-019-0324-8.

(25) Aufdenkampe, A. K.; Mayorga, E.; Raymond, P. A.; Melack, J. M.; Doney, S. C.; Alin, S. R.; Aalto, R. E.; Yoo, K. Riverine Coupling of Biogeochemical Cycles between Land, Oceans, and Atmosphere. *Front. Ecol. Environ.* **2011**, *9* (1), 53–60. https://doi.org/10.1890/100014.

(26) Bertagni, M. B.; Porporato, A. The Carbon-Capture Efficiency of Natural Water Alkalinization: Implications For Enhanced Weathering. *Sci. Total Environ.* **2022**, *838*, 156524. https://doi.org/10.1016/j.scitotenv.2022.156524.

(27) Calabrese, S.; Wild, B.; Bertagni, M. B.; Bourg, I. C.; White, C.; Aburto, F.; Cipolla, G.; Noto, L. V.; Porporato, A. Nano- to Global-Scale Uncertainties in Terrestrial Enhanced Weathering. *Environ. Sci. Technol.* **2022**, *56* (22), 15261–15272. https://doi.org/10.1021/acs.est.2c03163.

(28) Ho, D. T.; Bopp, L.; Palter, J. B.; Long, M. C.; Boyd, P. W.; Neukermans, G.; Bach, L. T. Monitoring, Reporting, and Verification for Ocean Alkalinity Enhancement. *State Planet* **2023**, *2-oae2023*, 1–12. https://doi.org/10.5194/sp-2-oae2023-12-2023.

(29) Subhas, A. V.; Rheuban, J. E.; Wang, Z. A.; McCorkle, D. C.; Michel, A. P. M.; Marx, L.; Dean, C. L.; Morkeski, K.; Hayden, M. G.; Burkitt-Gray, M.; Elder, F.; Guo, Y.; Kim, H. H.; Chen, K. A Tracer Study for the Development of In-Water Monitoring, Reporting, and Verification (MRV) of Ship-Based Ocean Alkalinity Enhancement. *Biogeosciences* **2025**, *22* (19), 5511–5534. https://doi.org/10.5194/bg-22-5511-2025.

(30) Szramek, K.; Walter, L. M. Impact of Carbonate Precipitation on Riverine Inorganic Carbon Mass Transport from a Mid-Continent, Forested Watershed. *Aquat. Geochem.* **2004**, *10* (1–2), 99–137. https://doi.org/10.1023/B:AQUA.0000038960.63501.5b.

(31) Gao, Y.; Jia, J.; Lu, Y.; Sun, K.; Wang, J.; Wang, S. Carbon Transportation, Transformation, and Sedimentation Processes at the Land-River-Estuary Continuum. *Fundam. Res.* **2024**, *4* (6), 1594–1602. https://doi.org/10.1016/j.fmre.2022.07.007.

(32) Tian, M.; Hartmann, J.; Suitner, N.; Amann, T.; Kempe, S.; Lim, C.; Moras, C. A. Stability of Alkalinity in the Land-Ocean Transition Zone: A Geochemical CDR Perspective for the Elbe River, Germany. *Environ. Res. Lett.* **2025**, *20* (9), 094053. https://doi.org/10.1088/1748-9326/adeeab.

(33) Rieder, L.; Hagens, M.; Poetra, R.; Vidal, A.; Calogiuri, T.; Neubeck, A.; Singh, A.; Corbett, T.; Niron, H.; Vicca, S.; Vlaeminck, S. E.; Janssens, I.; Verdonck, T.; Janssens, I.; Li, X.; Hammes, J. S.; Hartmann, J. Contribution of Dissolved Organic Carbon to Total Alkalinity in Enhanced Weathering Experiments. *Appl. Geochem.* **2026**, *198*, 106685. https://doi.org/10.1016/j.apgeochem.2026.106685.

(34) He, J.; Tyka, M. D. Limits and CO_2 Equilibration of Near-Coast Alkalinity Enhancement. *Biogeosciences* **2023**, *20* (1), 27–43. https://doi.org/10.5194/bg-20-27-2023.

(35) Da, F.; Stock, C. A.; Dunne, J. P.; Liu, X.; Luo, J. Y.; Lee, M.; Shevliakova, E. A Global Perspective on River Alkalinity: Drivers and Implications for Coastal Ocean Carbonate Chemistry. *Glob. Biogeochem. Cycles* **2025**, *39* (11). https://doi.org/10.1029/2025gb008528.

(36) Hessen, D. O.; Hindar, A. *Opptak Og Utslipp Av CO2 i Norske Vassdrag: En Empirisk Og Teoretisk Beregning [Uptake and Emission of CO2 in Norwegian Watercourses: An Empirical and Theoretical Calculation]*; Statens forurensningstilsyn (SFT), 1993.

(37) Hesthagen, T.; Sevaldrud, I. H.; Berger, H. M. Assessment of Damage and Loss of Fish Populations in Norwegian Lakes Due to Acidification. *Ambio* **1999**, *28* (2), 112–117.

(38) Sandøy, S.; Romundstad, A. J. Liming of Acidified Lakes and Rivers in Norway. *Water. Air. Soil Pollut.* **1995**, *85* (2), 997–1002. https://doi.org/10.1007/bf00476960.

(39) Rosseland, B. O.; Hindar, A. Liming of Lakes, Rivers and Catchments in Norway. *Water. Air. Soil Pollut.* **1988**, *41* (1–4), 165–188. https://doi.org/10.1007/BF00160350.

(40) Clair, T. A.; Hindar, A. Liming for the Mitigation of Acid Rain Effects in Freshwaters: A Review of Recent Results. *Environ. Rev.* **2005**, *13* (3), 91–128. https://doi.org/10.1139/a05-009.

(41) West, T. O.; McBride, A. C. The Contribution of Agricultural Lime to Carbon Dioxide Emissions in the United States: Dissolution, Transport, and Net Emissions. *Agric. Ecosyst. Environ.* **2005**, *108* (2), 145–154. https://doi.org/10.1016/j.agee.2005.01.002.

(42) Kaste, Ø. *Baseline pH Targets for Liming in the Kvina River*; Norwegian Institute for Water Research (NIVA), 2001.

(43) Jones, S. F.; Duke, P. J.; Manning, C. C. M.; Alexander, A.; Gonski, S. F.; Else, B. G. T. Lateral and Air-Water Inorganic Carbon and Methane Fluxes in a Small Arctic River: Seasonal Variations and the Connections with Local Hydrology. *Sci. Total Environ.* **2025**, *1002*, 180556. https://doi.org/10.1016/j.scitotenv.2025.180556.

(44) Wagner, R. J.; Boulger, R. W.; Oblinger, C. J.; Smith, B. A. *Guidelines and Standard Procedures for Continuous Water-Quality Monitors: Station Operation, Record Computation, and Data Reporting*, Version 1.0.; U.S. Geological Survey Techniques and Methods; Techniques and Methods 1-D3; U.S. Geological Survey: Reston, VA, 2006. https://doi.org/10.3133/tm1D3.

(45) Parkhurst, D. L.; Appelo, C. A. J. Description of Input and Examples for PHREEQC Version 3: A Computer Program for Speciation, Batch-Reaction, One-Dimensional Transport, and Inverse Geochemical Calculations, 2013. https://doi.org/10.3133/tm6A43.

(46) Gunning, P. J.; Hills, C. D.; Carey, P. J. Accelerated Carbonation Treatment of Industrial Wastes. *Waste Manag.* **2010**, *30* (6), 1081–1090. https://doi.org/10.1016/j.wasman.2010.01.005.

(47) Skjelvan, I.; Omar, A.; Kristensen, T. ICOS OTC SOOP Release from G.O. Sars, 2025-12-06–2025-12-17, 2025. https://hdl.handle.net/11676/PJYEFd2h6AvRt3weOznuj0hH.

(48) Hruška, J.; Köhler, S.; Laudon, H.; Bishop, K. Is a Universal Model of Organic Acidity Possible: Comparison of the Acid/Base Properties of Dissolved Organic Carbon in the Boreal and Temperate Zones. *Environ. Sci. Technol.* **2003**, *37* (9), 1726–1730. https://doi.org/10.1021/es0201552.

(49) Newcombe, C. P.; Macdonald, D. D. Effects of Suspended Sediments on Aquatic Ecosystems. *North Am. J. Fish. Manag.* **1991**, *11* (1), 72–82. https://doi.org/10.1577/1548-8675(1991)011%3C0072:EOSSOA%3E2.3.CO;2.

(50) Kemp, P.; Sear, D.; Collins, A.; Naden, P.; Jones, I. The Impacts of Fine Sediment on Riverine Fish. *Hydrol. Process.* **2011**, *25* (11), 1800–1821. https://doi.org/10.1002/hyp.7940.

(51) Gomez, F. A.; Wanninkhof, R.; Barbero, L.; Lee, S. Increasing River Alkalinity Slows Ocean Acidification in the Northern Gulf of Mexico. *Geophys. Res. Lett.* **2021**, *48* (24). https://doi.org/10.1029/2021GL096521.

(52) European Parliament; Council of the European Union. *Directive 2000/60/EC Establishing a Framework for Community Action in the Field of Water Policy*; 2000; Vol. L 327, pp 1–73. https://eur-lex.europa.eu/eli/dir/2000/60/oj.

(53) Direktoratsgruppen vanndirektivet. *Veileder 02:2018: Klassifisering av miljøtilstand i vann: Økologisk og kjemisk klassifiseringssystem for kystvann, grunnvann, innsjøer og elver*. https://www.statsforvalteren.no/siteassets/fm-agder/dokument-agder/miljo-og-klima/mudrin

g-utfylling-og-dumping/2018---02-veileder-klassifisering-av-miljotilstand-i-vann-27.10.20-1.pdf.

(54) Wetzel, R. G. *Limnology: Lake and River Ecosystems (3rd Ed.)*; Academic Press, 2001.

(55) Dodds, W. K.; Smith, V. H. Nitrogen, Phosphorus, and Eutrophication in Streams. *Inland Waters* **2016**, *6* (2), 155–164. https://doi.org/10.5268/IW-6.2.909.

(56) U.S. Environmental Protection Agency. *Aquatic Life Ambient Water Quality Criteria for Ammonia – Freshwater 2013*; U.S. Environmental Protection Agency, 2013. https://www.epa.gov/wqc/aquatic-life-criteria-ammonia.

(57) Neumann, R. B.; Kukla, T.; Zhang, S.; Butman, D. E. Riverine Photosynthesis Influences the Carbon Sequestration Potential of Enhanced Rock Weathering. *Front. Clim.* **2025**, *7*. https://doi.org/10.3389/fclim.2025.1582786.

(58) Saccardi, B.; Brinkerhoff, C. B.; Gleason, C. J.; Winnick, M. J. Toward Modeling Continental‐Scale Inland Water Carbon Dioxide Emissions. *AGU Adv.* **2024**, *5* (6). https://doi.org/10.1029/2024AV001294.

Table of Contents Graphic

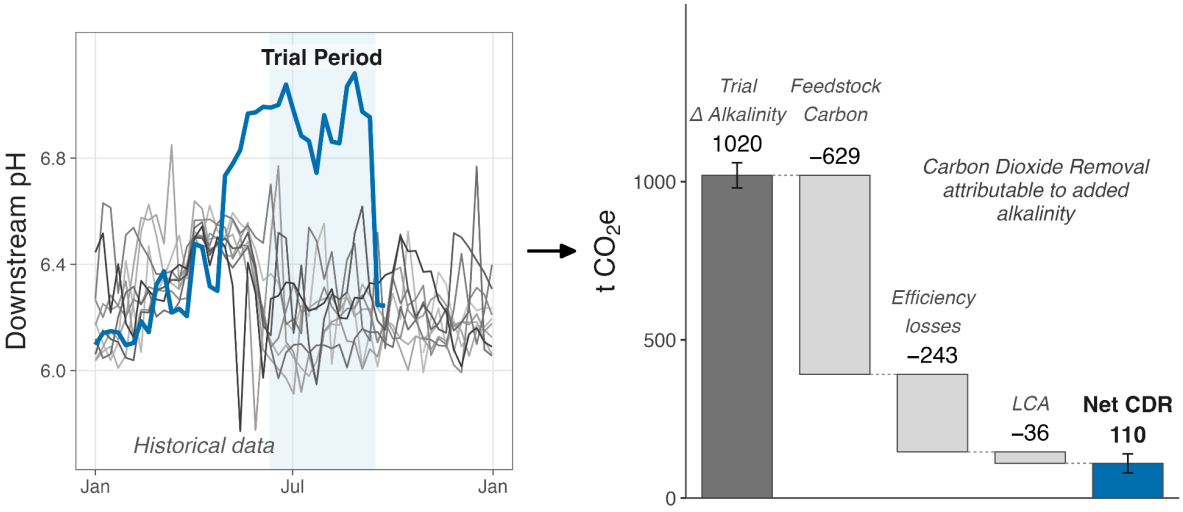

Supporting Information for:

Quantified Carbon Dioxide Removal from an Alkalinity Addition Field Trial in the Kvina River, Norway

Isaac W. R. Bahler[1,2], Benjamin F. Trueman[2], Rolf D. Vogt[3], Jack R. Tucker[2], Catherine E. Brenan[2], Shannon M. Sterling[1,2]*

Number of pages: 28 Figures: 1 Tables: 9

Table of Contents

1. Watershed characteristics for Litleåne and Kvina (pre- and post-diversion)

Prior to the Tonstad hydroelectric diversion in 1968, the Kvina catchment drained 1,445 km^2; Table S1). Hydropower agencies currently are required to maintain a minimum discharge of ~5 $m^3\ s^{-1}$.

Table S1. Comparison of catchment characteristics for the Litleåne and Kvina River (above dosers), with points of interest (POIs) used to delineate the catchments at the Nyland doser and river mouth.[a]

Watershed Characteristic	Litleåne above the doser Steindør	Kvina above the doser at Nyland (NY), post-diversion	Kvina watershed at the mouth (KL), pre-diversion
Area (km^2)	230	304	1445 (809)[b]
Elevation range (m a.s.l.)	9 – 876	0–427	0–1431
Lake (%)	6.8	6.1	14.1
Forest (%)	60.7	41.8	13.7
Agric. (%)	2	1.8	0.5
Bog (%)	7	5.2	3.1
Mountain (%)	11	35.1	65.6
Urban (%)	0.2	0	0
Other (%)	12.4	9.6	2.9
Temp (°C)	3.9	0.8	1.6
Precip (mm)	1781	1539	1605
ANC (µeq/L)	20	–	28
pH	5.0	5.3	5.5
TOC (mg C L^{-1})	8.5	5.7	6.6

[a] For the river mouth (KL), the value in parentheses is the post-diversion watershed area.

[b] Watershed areas are from Miljødirektoratet, 2002[1]

2. Water Chemistry Data Collection and Analytical Methods

In-situ sensor calibration. pH using two-point calibration with NIST-traceable buffer solutions (pH 4.01, 7.01) at field temperature conditions, and conductivity sensors with a similar two-point (μS cm^{-1} 84, 1413) potassium chloride standard calibration. Prior to deployment, pCO_2 sensors were factory calibrated using 4–6 World Meteorological Organization (WMO)-traceable CO_2 standards and a linear calibration function. The trial period fell within the manufacturer-recommended 12–18 month recalibration interval; so, pCO_2 sensors were not recalibrated during the experiment.

Grab-sample collection and handling. Grab samples were collected from the main flow of the river, as close to the thalweg as practicable, using a motorized pump. Sampling tubing was flushed with river water before bottles were filled. Where required by the analytical method, samples were collected through a site-specific in-line 0.45 μm filter; bottles requiring unfiltered water were filled separately.[2] Bottles were filled from the bottom, with the filling tube kept below the water line, and overflowed by approximately 3 bottle volumes before sealing. All bottles were filled without headspace to minimize atmospheric gas exchange. Samples were stored cool and protected from light and were transferred to the contracted laboratory as soon as practicable after collection. Any grab-sample collection for parameters beyond the *business-as-usual* sampling conducted by Kvinesdal Kommune was subcontracted to an environmental consultant in Norway, Powafa.

Historical Data. Historical pH and alkalinity data used for the counterfactual scenario were analyzed by three contracted laboratories: NIVA (2011–2015), VestfoldLAB AS (2011, 2016–2020), and Eurofins Environment Testing Norway AS, Moss (2021–2024) – each following established Norwegian and ISO standards. For grab samples collected as part of *business-as-usual* monitoring during the trial period, Kvinesdal Kommune continued its regular water-chemistry monitoring, using Eurofins for laboratory analysis.

Table S2. Trial NIVA Grab Sample Analysis Methods [c]

Parameter	Analysis Method
Alkalinity (filtered)	Modified NS-EN ISO 9963-1:1996
Chloride	Modified NS-EN ISO 10304-1:2009 (Anions) & NS-EN ISO 14911:1999 (Cations)
Sulfate	Modified NS-EN ISO 10304-1:2009 (Anions) & NS-EN ISO 14911:1999 (Cations)
Nitrate	Modified NS-EN ISO 10304-1:2009 (Anions) & NS-EN ISO 14911:1999 (Cations)
Fluoride	Modified NS-EN ISO 10304-1:2009 (Anions) & NS-EN ISO 14911:1999 (Cations)
Phosphate	Modified NS 4724:1984
Colour (filtered)	Modified NS-EN ISO 7887:2011, Method C
pH & Temperature-Compensated pH	NS-EN ISO 10523:2012
Conductivity & Temp.-Compensated Conductivity	NS-ISO 7888:1993 (automatic correction)
Turbidity	Modified NS-EN ISO 7027:2016
Suspended Solids (TSS)	Modified NS 4733:1983
DOC & TOC	Modified NS-EN 1484:1997

[c] Historical data were analyzed using the same or comparable procedures

Dissolved Inorganic Carbon. DIC was not analyzed by NIVA; it was instead subcontracted to ALS Global (an ISO 17025–accredited laboratory). The filtered samples were shipped to ALS in brown glass bottles with cooling elements; no chemical preservatives were added. Samples were stored and transported in insulated boxes to maintain a stable temperature and were delivered to the postal service on the same day, as soon as fieldwork was complete.

3. Water chemistry and discharge: river mouth versus limed control

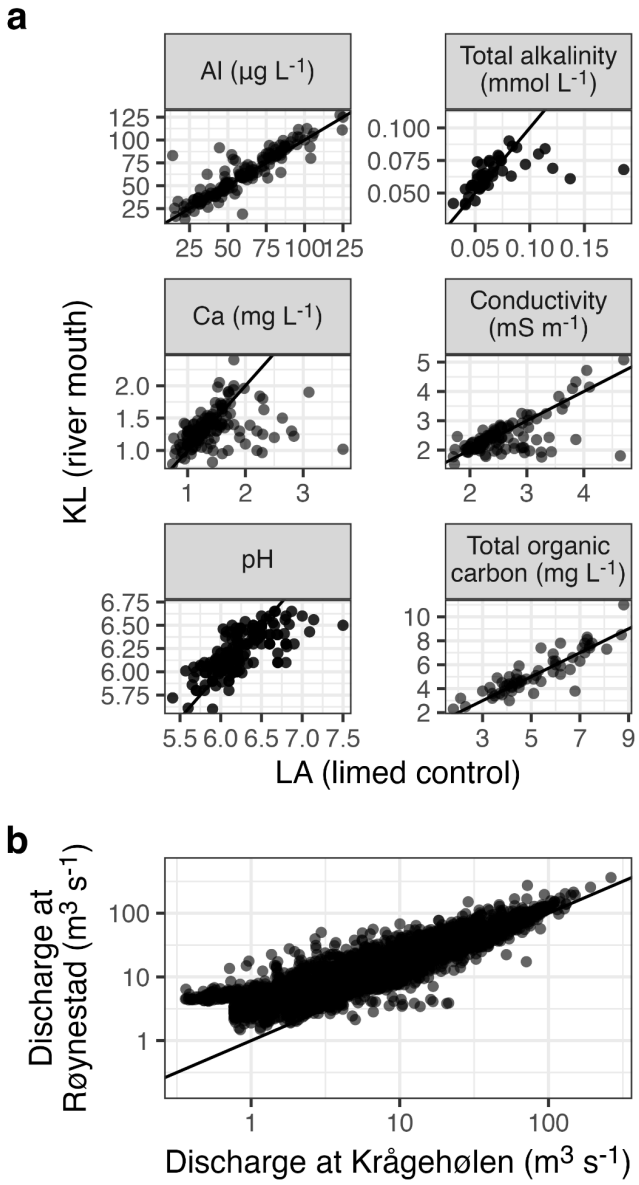

Figure S1. *Mainstem Kvina (KL) and Litleåne (LA) comparison.* ***(a).*** *Comparison of water chemistry at sites KL (river mouth) and LA (limed control).* ***(b)*** *Comparison of discharge at Norwegian Water Resources and Energy Directorate gauges on the Kvina mainstem (Røynestad) and the Litleåne tributary (Kragehølen).*

4. Kinetic modelling of calcite dissolution

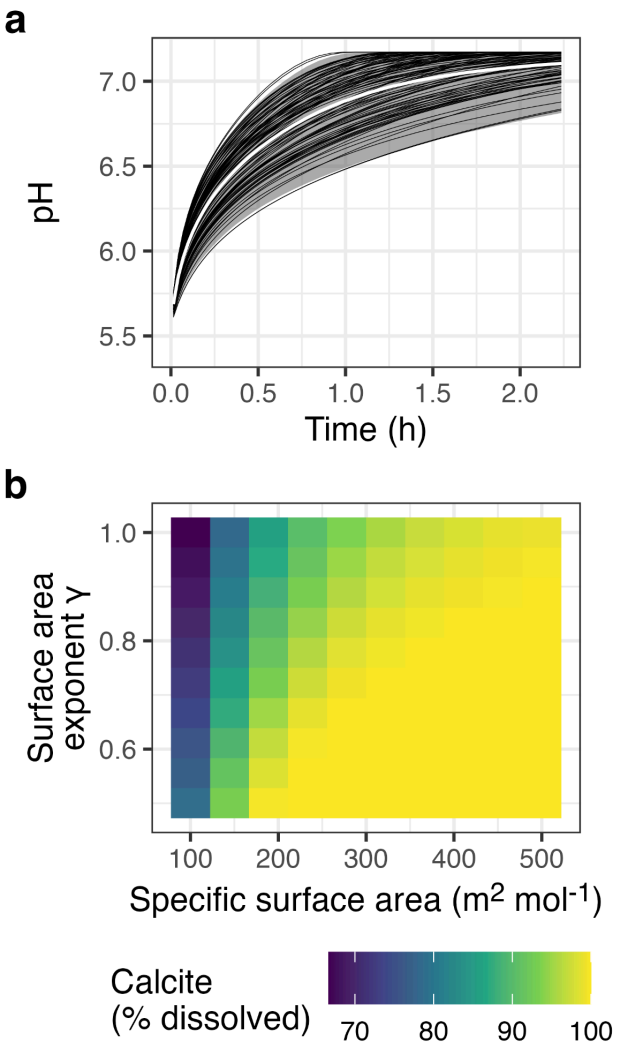

Figure S2. *Modelled kinetic calcite dissolution.* ***(a)*** *pH evolution with time under averaged Kvina River chemistry at site NY (upstream of the Nyland doser). Model runs were generated by a Monte Carlo simulation with 1000 parameter combinations (surface area 100–500 m² mol^{-1}; the calcite saturation-state inhibition exponent γ =(0.5–1.0).* ***(b)*** *Percent calcite dissolution as a function of specific surface area and the surface area exponent.*

5. Feedstock Characterization for the Potential CDR Estimate

Project feedstock consisted of Biokalk 75 produced at Omya Hustadmarmor AS's Elnesvågen facility from high-grade calcite marble sourced from Brønnøy and Hustadvika, Norway. Project-specific characterization was based on a single feedstock sample collected by Omya at the Elnesvågen plant and analyzed using microwave digestion with ICP-OES and ICP-MS, together with X-ray fluorescence. These complementary methods characterized the necessary constituents for the calculation of the feedstock's CO_2-removal potential from its bulk elemental and oxide composition. The source deposits occur within high-grade Caledonian metamorphic terranes and are dominated by coarse-grained, high-purity calcite marble with only minor dolomite and silicate impurities.[3] Although the project-specific analysis was limited to a single sample, its calcite content (trial sample of 96.5 wt% $CaCO_3$) was consistent with historical characterizations conducted between 2011 and 2020 (n = 5), which averaged 95.97 wt% by XRD (SD = 0.264%) and 94.41 wt% by XRF (SD = 0.490%).

Table S3. Atomic/molar masses of the constituent elements and the air–sea CO_2 retention efficiency (η_{ocean}) applied in the calculation.

Parameter	Value (g mol^{-1})
M_{Ca}	40.08
M_{Mg}	24.31
M_{Na}	22.99
M_{K}	39.10
M_{S}	32.07
M_{P}	30.97
M_{O}	16.00
M_{C}	12.01
β (unitless)	0.72

Table S4. Chemical (oxide) composition of the calcite feedstock determined by X-ray fluorescence (XRF), inductively coupled plasma optical emission spectroscopy (ICP-OES), and combustion with infrared (IR) detection; the mean is used in the calculation.

Oxide	XRF (% weight)	ICP-OES (% weight)	Combustion with IR (% weight)	Mean (% weight)
CaO	53.1	52.33	–	52.71
MgO	0.87	0.80	–	0.83
Na_2O	0.16	0.19	–	0.18
K_2O	0.08	0.37	–	0.23
SO_4 [d]	0.05	0.07	0.03	0.049
P_2O_5	0.02	0.01	–	0.015
C (inorganic)	–	–	11.94	11.94

[d] The SO_4 value is the mean of the elemental S concentration from ICP-OES, the SO_3 concentration from XRF, and the total S from combustion with IR detection.

Table S5. Feedstock CO_2-removal potential under the mean and conservative compositions, and at an air–sea CO_2 retention efficiency of 1 (undiscounted theoretical maximum).

Method	CO_2-removal potential (kg CO_2 t^{-1} feedstock)	CO_2-removal potential (t CO_2 t^{-1} feedstock)
Mean	307.22	0.307
Conservative [e]	305.94	0.306
Air–sea CO_2 retention efficiency of 1	424.92	0.425

[e] The conservative method uses the lower observed weight % for CaO, MgO, Na2O and K2O, and the higher observed weight % for SO_4 and P_2O_5.

Table S6. Conversion factor from mass calcite feedstock to moles of C

Parameter	Value (mol kg^{-1})
α [f]	9.941

[f] Calculated as ($C_{inorganic}$ / 100) *($M_C \cdot 1000$)

6. Quantification of Ocean Re-equilibration Losses

Ocean losses are accounted for in the "ocean loss" term when calculating both CO_2e stored and CO_2e counterfactual. These losses of CO_2 are due to re-equilibration of DIC upon discharge to the ocean. Ocean loss due to re-equilibration is accounted for using the retention efficiency equation 11 from Renforth and Henderson (2017)[4]:

$$\eta_{oceanlosses} = \frac{\Delta DIC_{T,Ocean}}{\Delta Alk_{T,Ocean}} = (S * 10^{-3.009} + 10^{-1.519}) * ln(pCO_2) - (S * 10^{-2.100}) - (T * pCO_2)(S * 10^{-7.501} - 10^{-5.598}) - (T * 10^{-2.337}) + 10^{0.102} \quad (1)$$

The Renforth and Henderson factor was calculated using sea-surface temperature, salinity, and pCO_2 data from approximately three years of releases from the Integrated Carbon Observation System Ocean Thematic Centre Ship of Opportunity Programme, collected aboard the G.O. Sars research vessel.[5] Across the period covered by these data, η_{Ocean} ranged from 0.81 to 0.91, with a mean value of 0.86 (Figure S3).

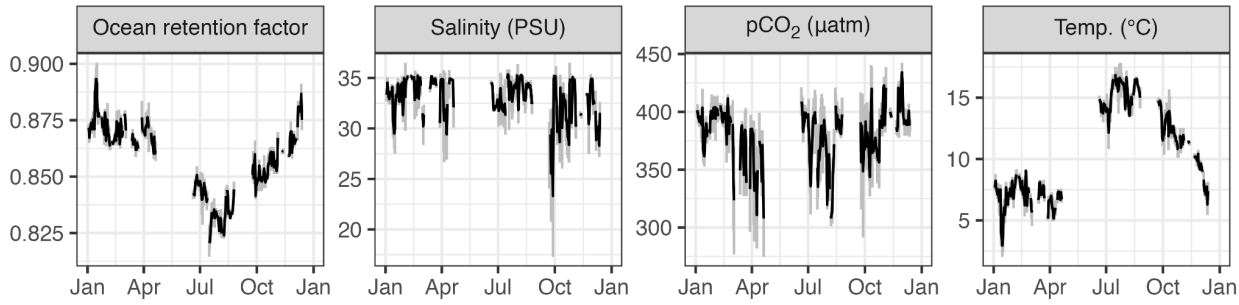

Figure S3. *Ocean retention factors and the inputs used to calculate them, averaged by ordinal day. Error bars (light grey) span one standard deviation about the mean.*

7. Life-cycle assessment emissions inventory

The certified carbon accounting data, which includes all assumptions, emission factors, proxies and environmental product declarations used to complete the LCA, are publicly accessible via the Isometric Registry (https://isometric.com/).

Table S7. Life cycle assessment (LCA) components and component emissions.

Component Group	**Activities and Processes included in Group (Component Emissions)**	**Total tCO_2e**
Calcite feedstock manufacturing and transport	Feedstock Sourcing and Processing (21.4 tCO_2e) Feedstock Transport (13.2 tCO_2e)	3.46×10^{1}
Energy Use	Electricity Use at Doser (0.139 tCO_2e)	1.39×10^{-1}
Project emissions	Staff Travel (0.595 tCO_2e) Sensors (0.120 tCO_2e)	7.15×10^{-1}
Sampling and MRV	Field Team Transport (0.152 tCO_2e) Grab Sample Consumables (0.085 tCO_2e) Grab Sample Processing (0.076 tCO_2e) Grab Sample Shipping (0.069 tCO_2e)	3.83×10^{-1}
Total Operational Lifecycle Emissions		35.9

8. Counterfactual Weathering of Feedstock

Because Biokalk 75 is a by-product that would otherwise have been discharged with calcite tailings to the Hustadmarmor submarine tailings deposit in Frænfjorden, we deducted the carbon dioxide uptake expected under this counterfactual fate from Gross CDR. We estimated counterfactual weathering through three pathways: (i) advective transport and dissolution of fine particles, (ii) dissolution of settled tailings, and (iii) dissolution before discharge.

For advective transport, we conservatively assumed that 10 % of the total tailings mass bypassed the primary settling plume, remained suspended as fine particles, dissolved, and fully equilibrated with the atmosphere. This assumption effectively treats all discharged material as available to enter the secondary plume before applying the 10 % advected-fines fraction, although field observations indicate that most material settles rapidly near the discharge point and that some advected fines also settle at distance.[6,7] For dissolution of settled tailings, PHREEQC calculations indicated that bulk fjord water remained supersaturated with respect to calcite; we therefore considered abiotic dissolution negligible. We nevertheless modelled organic-matter-driven dissolution using reactive transport simulations. The model assumed that deposited tailings remained reactive for 100 years despite deposition rates of 1–2.5 m yr^{-1}, that all dissolution products escaped pore waters and equilibrated with the atmosphere, and that reprecipitation did not offset dissolution.[8–10] We also used an intentionally high sediment organic-carbon content of 2.5 % by dry mass. This value was derived by tripling the mean of available measurements and may overestimate metabolically driven dissolution because incomplete removal of inorganic carbon can bias organic-carbon analyses upward in calcite-rich sediments.[11,12,9] Finally, we modelled dissolution before discharge under deliberately acidic freshwater conditions (pH 5; pCO_2 = 1,000 μatm), representing a conservative upper-bound scenario (the fresh process water used in the plant is from a circumneutral pH lake).

The final counterfactual weathering deduction was 100.1 t CO_2e. For the 1480 t feedstock counterfactual scenario, the 96 % fraction of feedstock smaller than 10 μm was matched to the 60 % <10 μm fraction of the receiving tailings, yielding a 2,368 t equivalent tailings discharge. We assumed that 10 % of this mass, or 237 t, was advected, dissolved, and generated 72.5 t CO_2e of uptake using a conservative feedstock CDR potential of 0.306 t CO_2e t^{-1}. The equivalent

tailings mass contained 1,421 t of calcite, of which 1,184 t was assumed to have settled. The reactive-transport model predicted dissolution of 7.6 % of this settled calcite, equivalent to approximately 90 t of calcite and 27.50 t CO_2e of uptake. Dissolution prior to discharge contributed a further 0.1 t CO_2e under the acidic-water assumption. Summing these terms – 72.5, 27.5, and 0.1 t CO_2e – gave the counterfactual-weathering of 100.1 t CO_2e.

9. Trial Statistical Comparison between NY and OB

Weekly grab samples were collected at NY and OB during the 10 June–15 September 2025 quantification window (n = 15 per station), except for dissolved oxygen (n = 2 per station) and filtered Ni at NY (n = 14). Reported means, sample standard deviations (SD), and statistical tests use all available observations. Cations, trace metals, alkalinity, DIC, DOC and Al were analyzed in the filtered (0.45 µm) fraction; major anions, total phosphorus, and Zn were unfiltered; and field parameters, ANC, and TOC were measured on whole samples. Values below detection were assigned the reported detection limit. NY and OB were compared using two-sided Welch t-tests at $\alpha = 0.05$ (with additional $\alpha = 0.01$ and $\alpha = 0.001$ reported where available) without multiple-comparison correction; degrees of freedom were estimated using the Welch–Satterthwaite approximation. The t-statistic was calculated as (mean NY − mean OB)/SE, such that negative values indicate lower concentrations at NY. We assumed that serial correlation among observations was negligible; p-values are underestimated to the extent that this assumption is false.

Table S8. Upstream (NY) vs downstream (OB) Welch t-tests

Parameter	Unit	Mean NY	SD NY	Mean OB	SD OB	t	df	p-value	Significance
pH	unitless	5.45	0.254	7.2	0.135	−23.6	21.3	9.7×10^{-17}	Significant
Conductivity	mS/m	2.1	0.357	3.67	0.441	−10.7	26.9	3.34×10^{-11}	Significant
Alkalinity (filtered)	mmol/L	4.65×10^{-2}	6.1×10^{-3}	0.205	3.21×10^{-2}	−18.8	15	7.53×10^{-12}	Significant
Acid neutralizing capacity (ANC)	µeq/L	29.5	7.31	217	44.3	−16.2	14.8	8.22×10^{-11}	Significant
Dissolved inorganic carbon (DIC)	mg L^{-1} C	0.962	0.543	2.27	1.27	−3.66	19	1.67×10^{-3}	Significant
Calcium (filtered)	mg L^{-1}	0.606	6.99×10^{-2}	4.28	0.756	−18.7	14.2	1.97×10^{-11}	Significant
Aluminum (reactive)[g]	µg L^{-1}	67.0	21.7	35.2	14.6	2.713	7.0	0.030	Significant
Phosphate (PO_4-P)	µg L^{-1} P	1.07	0.258	1.93	0.799	−4	16.9	9.41×10^{-4}	Significant
Cobalt (filtered)	µg L^{-1}	9.49×10^{-2}	3.16×10^{-2}	6.8×10^{-2}	3.25×10^{-2}	2.3	28	2.9×10^{-2}	Significant
Manganese (filtered)	µg L^{-1}	8.52	2.12	3.77	1.95	6.38	27.8	6.77×10^{-7}	Significant
Colour	mg L^{-1} Pt	49.9	25.1	57.6	29.2	−0.771	27.4	4.47×10^{-1}	Not significant

Parameter	Unit	Mean NY	SD NY	Mean OB	SD OB	t	df	p-value	Significance
Total suspended matter	mg L^{-1}	1.93	0.303	1.96	0.447	−0.21	24.6	8.35×10^{-1}	Not significant
Turbidity	FNU	0.734	0.133	0.843	0.256	−1.47	21.1	1.57×10^{-1}	Not significant
Total organic carbon (TOC, unfiltered)	mg L^{-1}	5.82	2.42	5.94	2.41	−0.136	28	8.93×10^{-1}	Not significant
Dissolved organic carbon (DOC)	mg L^{-1} C	5.69	2.39	5.83	2.37	−0.161	28	8.73×10^{-1}	Not significant
Magnesium (filtered)	mg L^{-1}	0.286	6.46×10^{-2}	0.317	6.99×10^{-2}	−1.28	27.8	2.12×10^{-1}	Not significant
Sodium (filtered)	mg L^{-1}	2.28	0.477	2.29	0.47	−0.081	28	9.36×10^{-1}	Not significant
Potassium (filtered)	mg L^{-1}	0.164	2.97×10^{-2}	0.165	3.18×10^{-2}	−0.119	27.9	9.06×10^{-1}	Not significant
Sulphate (unfiltered)	mg L^{-1}	0.827	0.114	0.834	0.114	−0.16	28	8.74×10^{-1}	Not significant
Chloride (unfiltered)	mg L^{-1}	3.92	0.821	3.97	0.789	−0.179	28	8.59×10^{-1}	Not significant
Fluoride	mg L^{-1}	4.03×10^{-2}	1.24×10^{-2}	4.25×10^{-2}	1.32×10^{-2}	−0.471	27.9	6.41×10^{-1}	Not significant
Nitrate (NO_3-N, unfiltered)	mg L^{-1}	1.95×10^{-2}	1.36×10^{-2}	2.69×10^{-2}	1.56×10^{-2}	−1.38	27.5	1.77×10^{-1}	Not significant
Total phosphorus (unfiltered)	mg L^{-1}	7.65×10^{-3}	1.76×10^{-3}	8.21×10^{-3}	1.94×10^{-3}	−0.818	27.7	4.2×10^{-1}	Not significant
Aluminum (filtered)	mg L^{-1}	0.177	8.41×10^{-2}	0.174	7.4×10^{-2}	0.101	27.6	9.2×10^{-1}	Not significant
Arsenic (filtered)	µg L^{-1}	0.166	9.32×10^{-2}	0.166	7.82×10^{-2}	0.017	27.2	9.87×10^{-1}	Not significant
Cadmium (filtered)	µg L^{-1}	2.23×10^{-2}	6.61×10^{-3}	1.84×10^{-2}	4.98×10^{-3}	1.81	26	8.19×10^{-2}	Not significant
Chromium (filtered)	µg L^{-1}	0.109	3.23×10^{-2}	0.11	3.31×10^{-2}	−0.055 8	28	9.56×10^{-1}	Not significant
Copper (filtered)	µg L^{-1}	3.23	1.25	3.06	1.19	0.384	27.9	7.04×10^{-1}	Not significant
Iron (filtered)	µg L^{-1}	155	73.6	158	66.6	−0.12	27.7	9.06×10^{-1}	Not significant
Nickel (filtered)	µg L^{-1}	0.201	5.72×10^{-2}	0.195	5.81×10^{-2}	0.303	26.9	7.64×10^{-1}	Not significant
Lead (filtered)	µg L^{-1}	0.475	0.264	0.421	0.235	0.589	27.6	5.61×10^{-1}	Not significant
Uranium (filtered)	µg L^{-1}	0.135	4.73×10^{-2}	0.143	4.43×10^{-2}	−0.499	27.9	6.22×10^{-1}	Not significant

Parameter	Unit	Mean NY	SD NY	Mean OB	SD OB	t	df	p-value	Significance
Vanadium (filtered)	µg L^{-1}	0.171	7.34×10^{-2}	0.184	6.54×10^{-2}	−0.512	27.6	6.12×10^{-1}	Not significant
Zinc (unfiltered)	µg L^{-1}	3.77	1.2	3.52	0.874	0.662	25.6	5.14×10^{-1}	Not significant

[g] Trial sampling included only filtered and unfiltered ICP-MS aluminum, neither of which was expected to show changes relevant to water-quality assessment. To supplement these data, reactive aluminum concentrations from NIVA's business-as-usual monthly monitoring at NY and KL rather than at NY and OB were compared during the trial period (n = 5 per station).

10. Seasonal Salt Signal Spike and Separation from the Trial Period

Because Mg, Na, and Cl concentrations all increased during the trial, further analysis was required to determine whether the apparent Mg response reflected the additional feedstock or broader seasonal hydrochemical variability. Observed Mg concentrations were compared with the values expected for each day of the year based on the 2011–2024 seasonal-GAM climatology, while the relative departures of Mg, Na, and Cl were evaluated together to identify common temporal behaviour (Figure S4a,b). Na and Cl provide useful indicators of broader salt inputs because neither was expected to respond materially to calcite addition. The complete 2025 records were subsequently examined to determine whether these anomalies were confined to the treatment period or formed part of a longer seasonal pattern (Figure S4c).

Mg closely covaried with Na and Cl, and substantial anomalies also occurred outside the trial period, including two pronounced early-winter events. This correspondence suggests that much of the Mg increase observed during the trial reflected a broader seasonal salt pulse rather than the alkalinity-addition treatment. A small proportion was nevertheless likely attributable to Mg contained in the additional feedstock.

Interpretation of the Ca record at LA required additional caution because no historical Ca measurements were available for that station. The upstream Litleåne climatology was therefore used as a reference, although it does not capture the expected downstream influence of routine liming. The historical GAM for KL, which is downstream of existing dosing operations, similarly shows Ca concentrations elevated relative to the upstream stations but does not exhibit the additional increase associated with enhanced dosing in 2025 (Figure S4c). Given the strong seasonal confounding identified for Mg, it was removed from Figure 2 to avoid presenting background hydrochemical variability as a treatment response and is instead reported here with the temporal context necessary for interpretation.

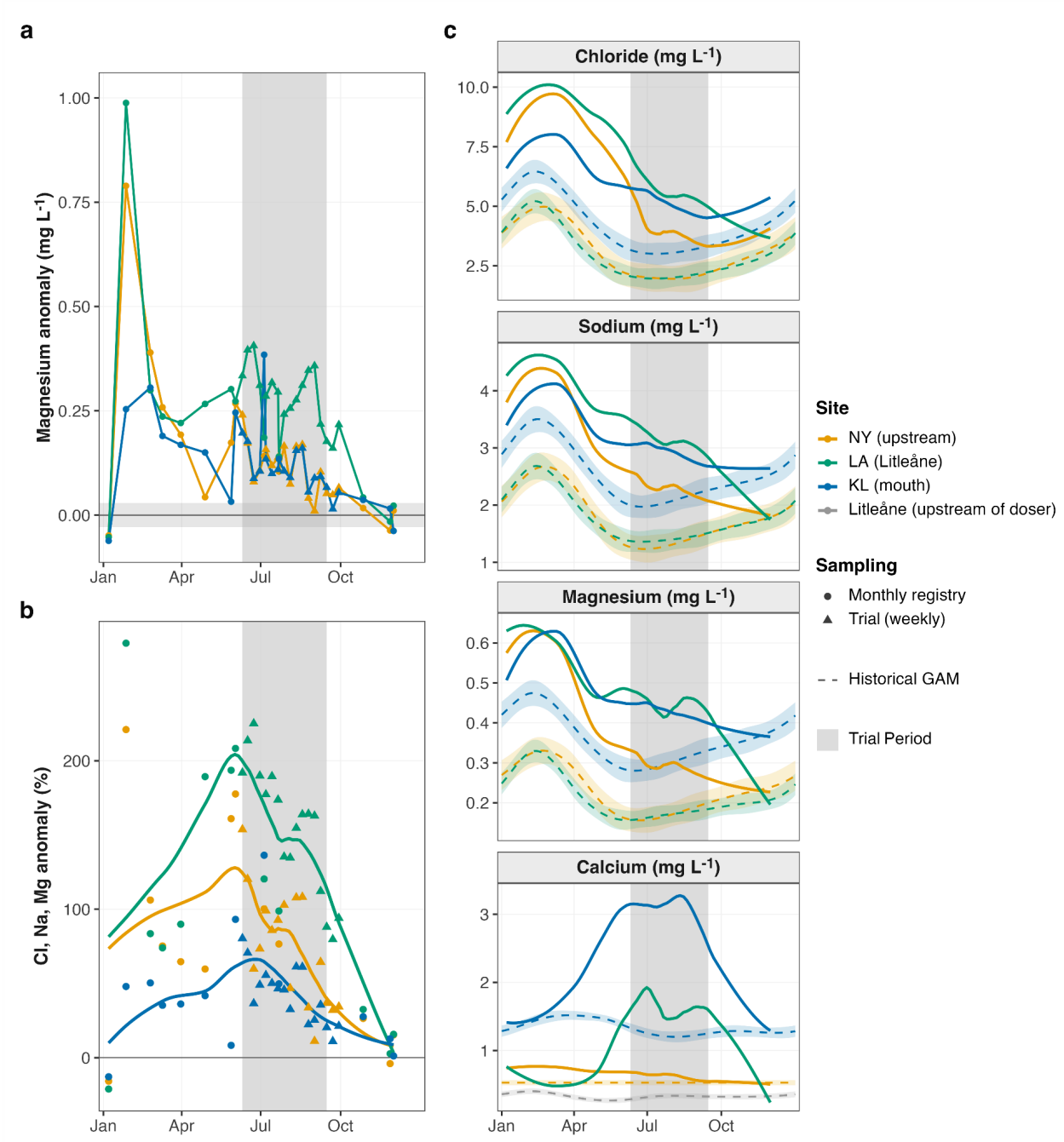

Figure S4. *Figure S4. Seasonal salt-tracer dynamics relative to the 2011–2024 baseline. Panels show* ***(a)*** *the absolute Mg anomaly relative to the seasonal-GAM baseline, with a ±2 SE envelope;* ***(b)*** *the 2025 LOESS trend in the mean relative anomaly of Cl, Na, and Mg; and* ***(c)*** *the raw 2025 Cl, Na, Mg, and Ca records over their respective seasonal-GAM climatologies. The grey vertical band denotes the trial period (10 June–15 September 2025).*

11. Historical Monthly Water-Chemistry Grab Samples (2011–2025)

Historical datasets were acquired from the national water database Vannmiljø (administered by the Norwegian Environment Agency). Records from 2011 to 2025 were evaluated at NY, Nyland upstream of the mainstem doser; KL, Kloster at the river mouth; LA, Litleåne før Kvina downstream of the tributary doser; and the Litleåne site upstream of the doser (Figures S5–S7). Colours consistently identify NY (orange), KL (dark blue), LA (green), and the upstream Litleåne site (grey). Lines connect routine observations only, exclude the additional grab samples collected during the 2025 trial, and are interrupted where sampling gaps exceed approximately six months; parameters are omitted where records are unavailable or too sparse for meaningful display. The shaded interval denotes the quantification period from 10 June to 15 September 2025.

Sulphate at KL during the trial remained below the full 2011–2024 baseline (1.07 vs 1.20 mg L^{-1}; $p < 0.01$), although the difference weakened when the comparison was restricted to 2020–2024, consistent with the long-term decline in sulphate deposition rather than a treatment effect. Nitrate at KL was likewise below its historical baseline (0.054 vs 0.099 mg N L^{-1}; $p < 0.001$) but increased through the trial along its typical seasonal trajectory (Figure S7). Mean TOC and total phosphorus at KL were statistically unchanged from historical conditions (5.64 vs 6.59 mg L^{-1} and 9.52 vs 8.79 µg P L^{-1}, respectively; $p > 0.05$), with total phosphorus remaining within the oligotrophic range. One anomalous total-phosphorus observation of approximately 92 µg P L^{-1} on 2 December 2024 was excluded from Figure S7 for axis legibility. In Figure S5, labile aluminum was calculated as reactive - non-labile aluminum; the directly reported 2016–2018 series matched this difference exactly ($r = 1.00$; median absolute difference approximately 0), supporting its derivation across the full record. LA is omitted from the ANC panel because no ANC record is available. In Figure S6, all four stations are shown for calcium and conductivity; LA is omitted from magnesium and chloride because these parameters are not reported and from potassium because only three observations are available. Station coverage in Figure S7 similarly varies with data availability, and LA is shown only for TOC.

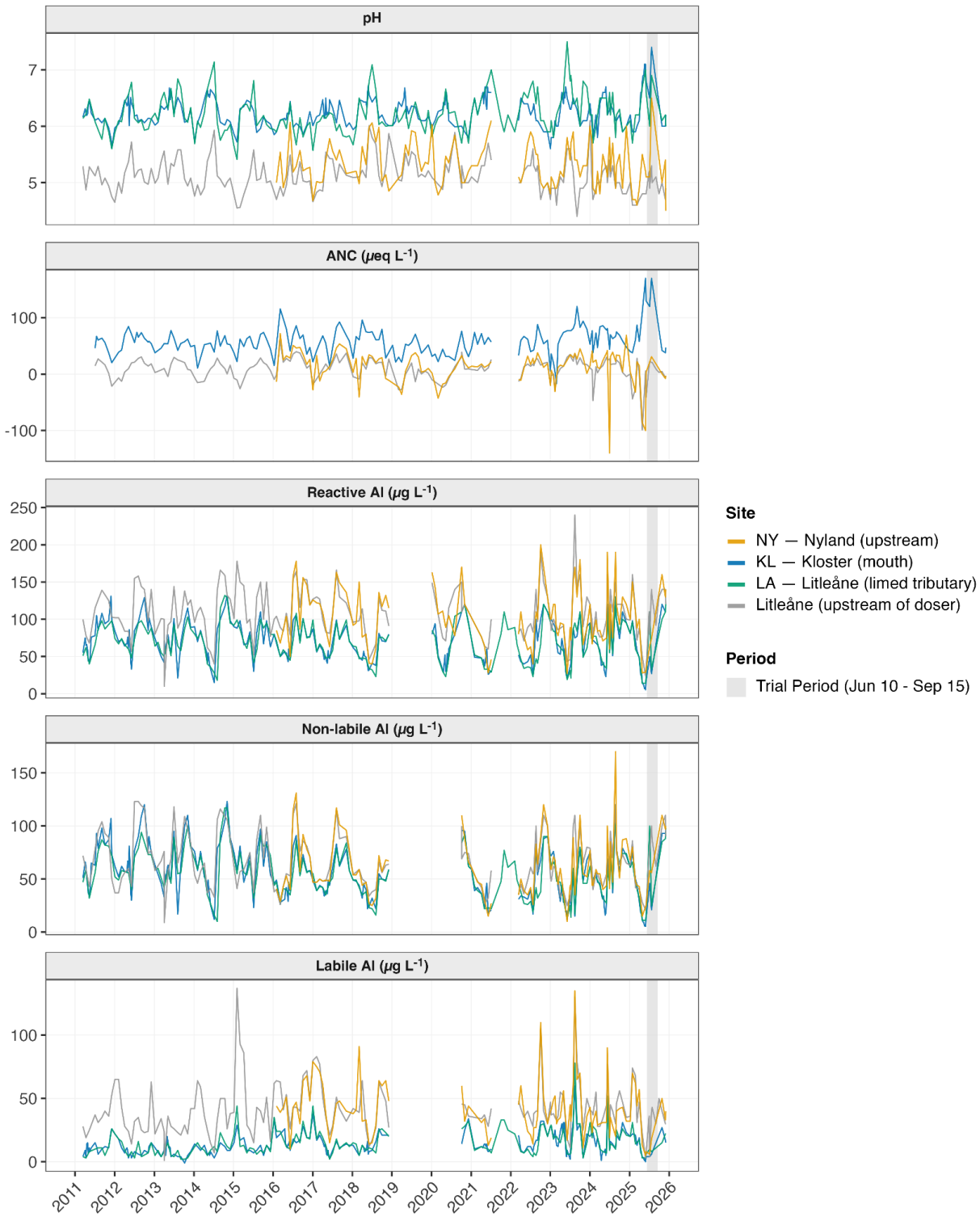

Figure S5. *Historical acidification and aluminum-fraction records within the Kvina River monitoring network, 2011–2025. Vertically stacked panels show pH, acid-neutralizing capacity (ANC), reactive aluminum, non-labile aluminum, and labile aluminum.*

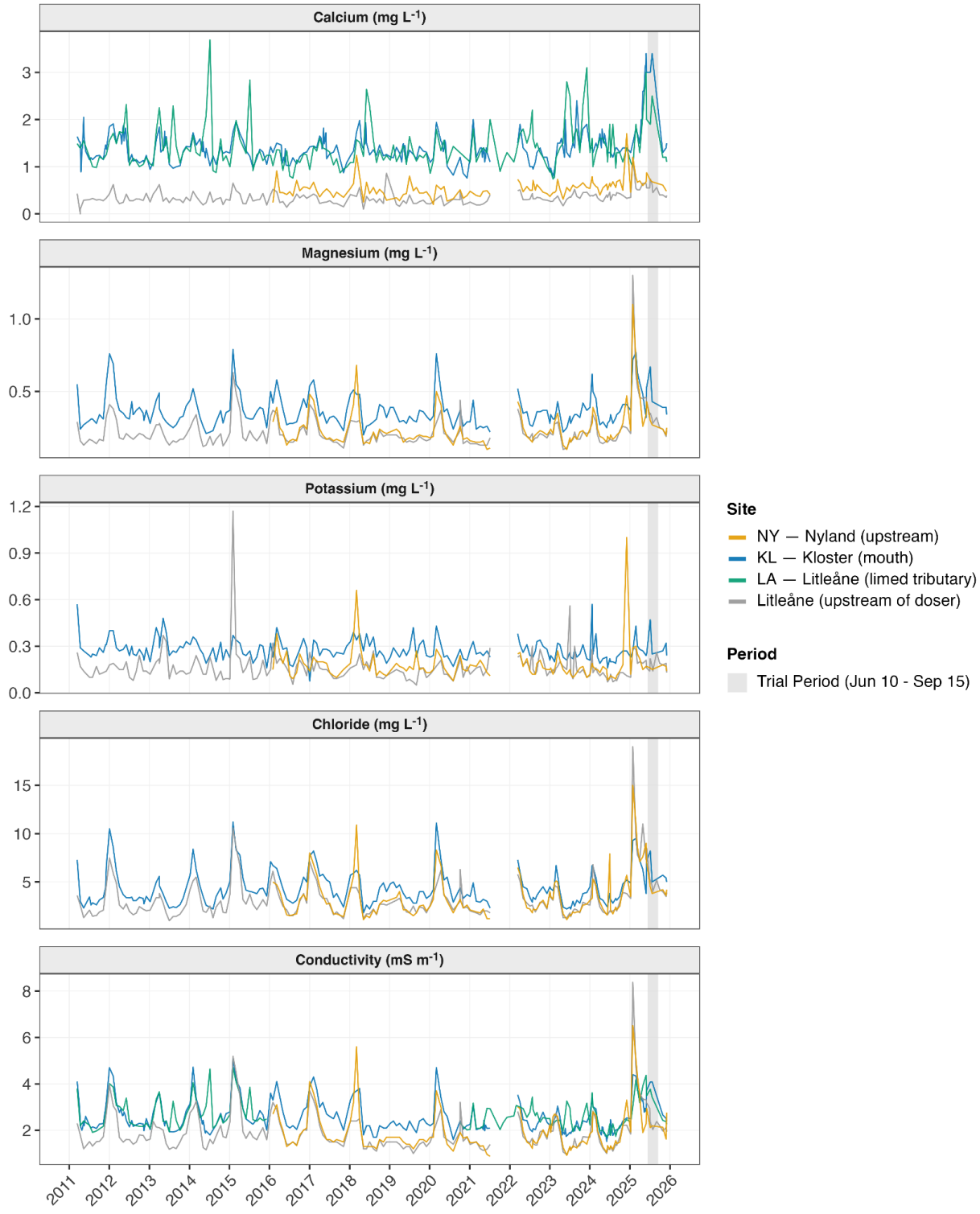

Figure S6. *Historical major-ion and conductivity records within the Kvina River monitoring network, 2011–2025. Vertically stacked panels show Ca, Mg, K, Cl, and conductivity. The 2025 Increases in calcium and conductivity at KL are consistent with liming-derived Ca^{2+}, whereas concurrent increases in sodium, chloride, and magnesium reflect seasonal variability.*

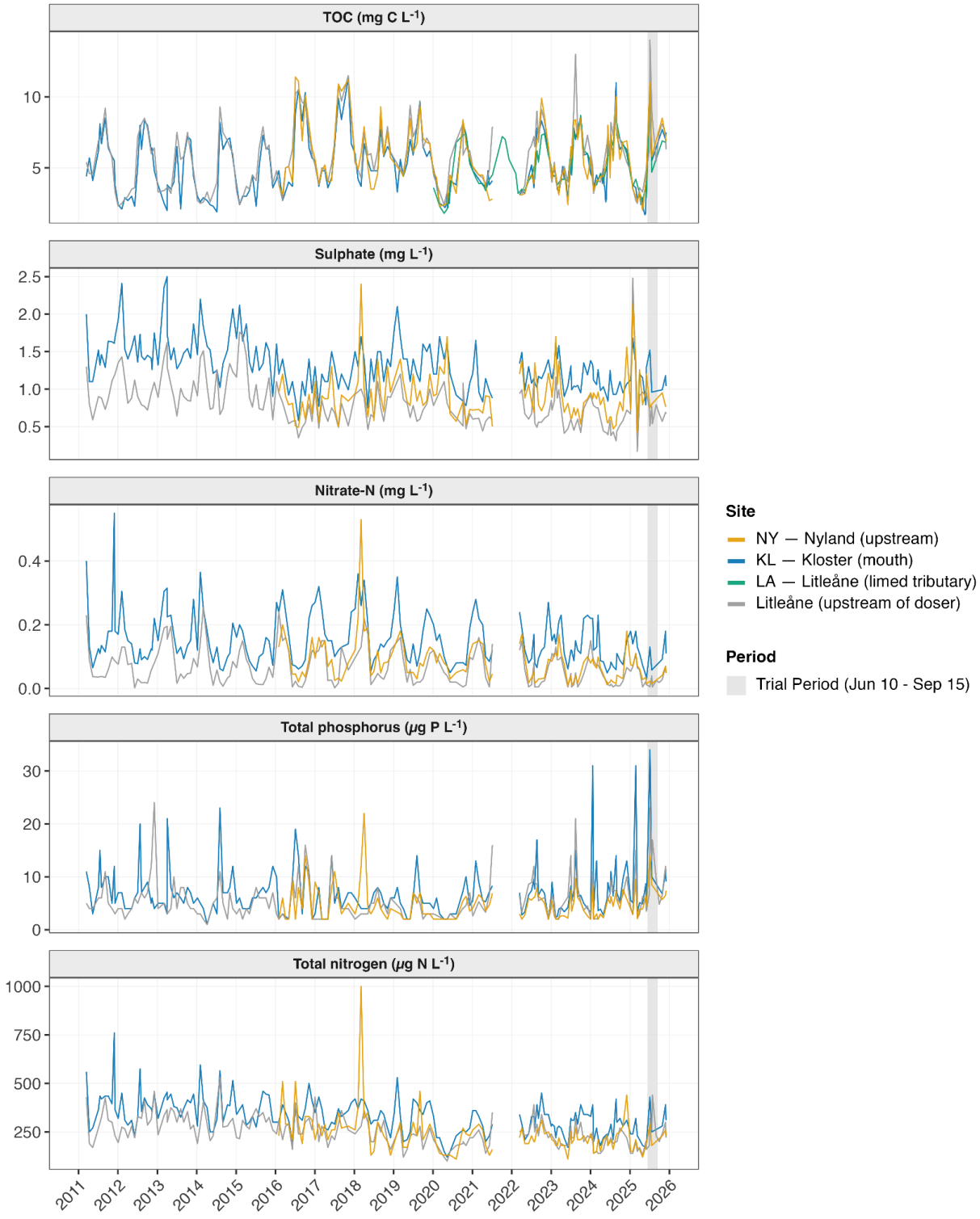

Figure S7. *Long-term nutrient and organic-carbon records within the Kvina monitoring network, 2011–2025. Vertically stacked panels show total organic carbon (TOC), sulphate, nitrate, total phosphorus, and total nitrogen. No clear liming response is evident in the nutrient or organic-carbon records.*

12. Trial Period Weekly Water-Chemistry Grab Samples (2025)

Weekly water-chemistry grab samples were collected by Powafa at NY, Nyland upstream of the mainstem doser; OB, 2.27 km downstream of the doser; KL, Kloster at the river mouth; LA, Litleåne før Kvina downstream of the tributary doser; and the Litleåne site upstream of the doser from 10 June to 15 September 2025 (Figures S5–S7). Colours consistently identify NY (orange), OB (light blue), KL (dark blue), LA (green), and the upstream Litleåne site (grey).

Lines connect successive samples, with consistent colours identifying the four monitoring sites across all panels. The dataset spans acidification indicators, major ions, conductivity, organic carbon, and nutrients, allowing temporal and spatial patterns to be compared among the upstream, immediately downstream, tributary-influenced, and river-mouth stations. Total aluminum in Figure S8 was measured by ICP-MS during the trial and is not directly comparable with the reactive, non-labile, and labile aluminum fractions in the historical monitoring record. Calcium and magnesium are shown as total, unfiltered concentrations to remain consistent with the corresponding Norwegian historical-monitoring measurements (Figure S9), and nitrate is expressed as NO_3^- –N in mg N L^{-1} (Figure S10). During the trial, sulphate and nitrate were significantly higher at KL than at NY, increasing from 0.827 to 1.07 mg L^{-1} and from 0.020 to 0.054 mg respectively (both $p < 0.001$), but neither parameter differed significantly between NY and OB ($p > 0.05$; Table S8, Figure S9). Nutrient concentrations generally increased during high-discharge events (Figure S10), and nitrate rose through the trial along the seasonal trajectory evident in the long-term record (Figure S7). These spatial and temporal patterns are more consistent with runoff-driven catchment export than with a treatment response. TOC and total phosphorus likewise showed no consistent treatment-related change. Collectively, the trial samples suggest that the treatment added carbonate alkalinity without measurably altering the river's organic-carbon or nutrient regime.

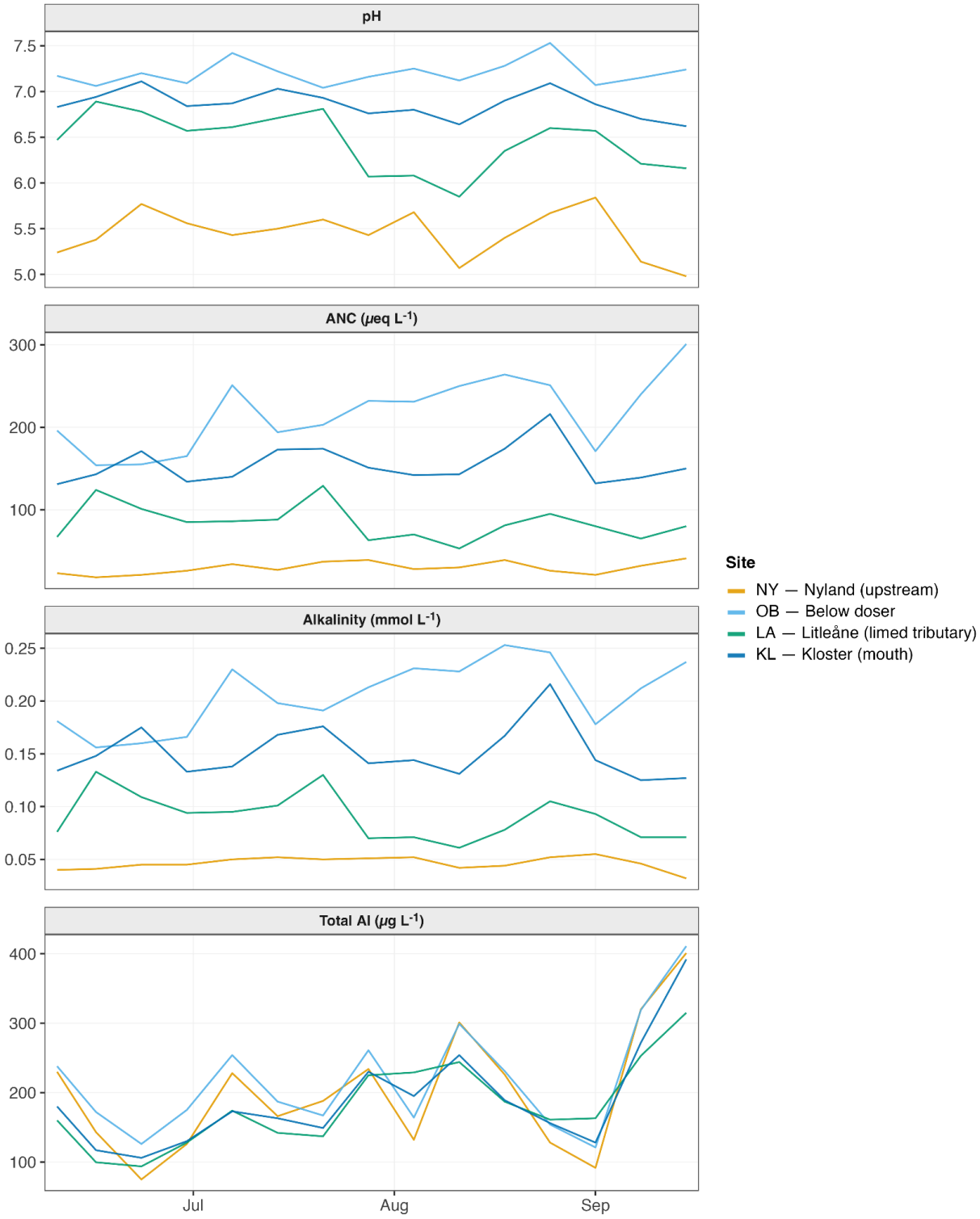

Figure S8. *Trial-period acidification and aluminum time series, 10 June–15 September 2025. Vertically stacked panels show pH, acid-neutralizing capacity (ANC), alkalinity, and total aluminum.*

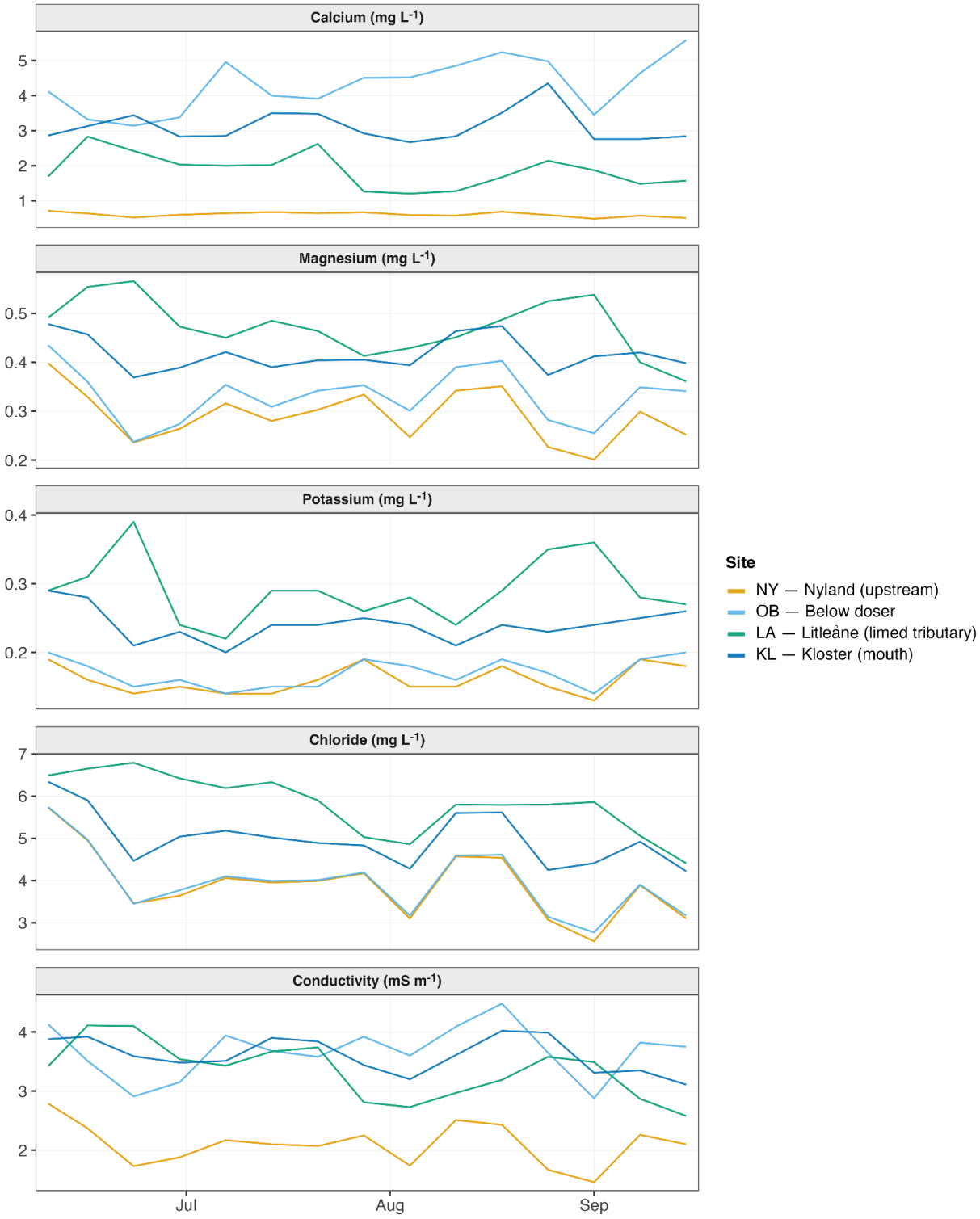

Figure S9. *Trial-period major-ion and conductivity time series, 10 June–15 September 2025. Vertically stacked panels show total calcium, total magnesium, potassium, chloride, and conductivity.*

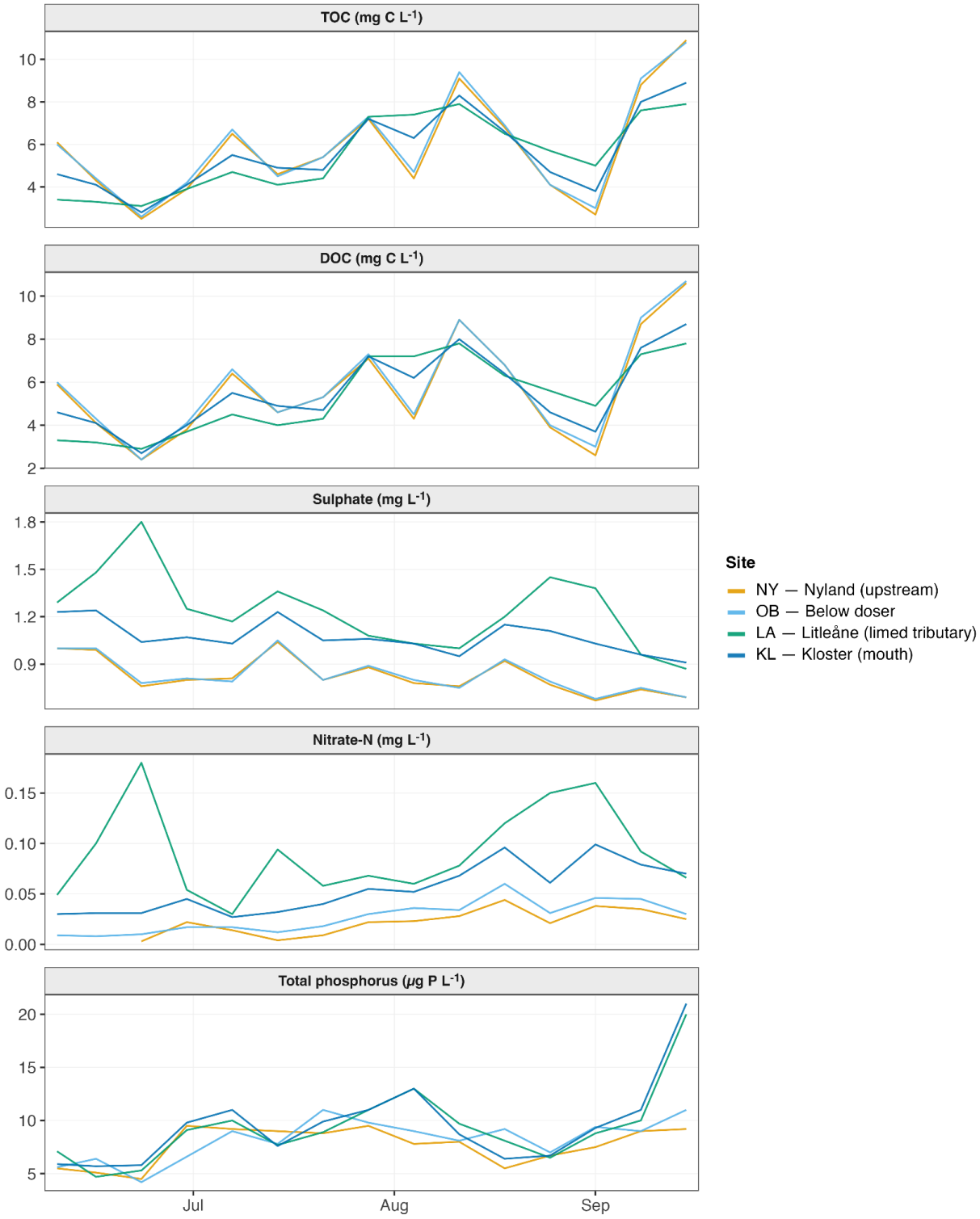

Figure S10. *Trial-period organic-carbon and nutrient time series, 10 June–15 September 2025. Vertically stacked panels show total organic carbon (TOC), dissolved organic carbon (DOC), sulphate, nitrate-N, and total phosphorus at NY, OB, LA, and KL.*

13. Ecological responses to pH elevation

Table S9. Potential ecological responses to pH elevation in freshwater systems relevant to river alkalinity enhancement (RAE).

Process	Mechanism	pH threshold	Consequence	Evidence	References
Phosphorus cycling	pH alters phosphate sorption on Fe/Al oxides; higher pH reduces sorption capacity	>7.5–8.5: initial shifts; >8.5 stronger	Increased dissolved P; potential productivity stimulation	Moderate–strong	[13,14]
Ammonia toxicity	pH shifts NH_4^+/NH_3 equilibrium toward un-ionised NH_3	<7.5: NH_3 very low; >8 rapid increase	Acute/chronic toxicity to fish where ammonium present	Very strong	[15,16]
Algal community	Elevated pH reduces dissolved CO_2; favours HCO_3^--utilising taxa	>8: alkaliphiles; >9: cyanobacterial risk in nutrient-rich systems	Community shift; cyanobacteria only in eutrophic conditions	Moderate	[13,17]

14. REFERENCES

(1) Miljødirektoratet. *Kvina – Konsekvenser Av Reguleringer*; Report N2002-1; Norwegian Environment Agency: Oslo, Norway, 2002. https://www.miljodirektoratet.no/globalassets/publikasjoner/dirnat/attachment/2197/n2002-1-kvina.pdf.

(2) Jones, S. F.; Duke, P. J.; Manning, C. C. M.; Alexander, A.; Gonski, S. F.; Else, B. G. T. Lateral and Air-Water Inorganic Carbon and Methane Fluxes in a Small Arctic River: Seasonal Variations and the Connections with Local Hydrology. *Sci. Total Environ.* **2025**, *1002*, 180556. https://doi.org/10.1016/j.scitotenv.2025.180556.

(3) Geological Survey of Norway. *Deposit 1551 - 303 Nås*. The Industrial Mineral Database. https://aps.ngu.no/pls/oradb/minres_deposit_fakta_NY.Main?p_objid=7827&p_spraak=E (accessed 2026-07-21).

(4) Renforth, P.; Henderson, G. Assessing Ocean Alkalinity for Carbon Sequestration. *Rev. Geophys.* **2017**, *55* (3), 636–674. https://doi.org/10.1002/2016RG000533.

(5) Skjelvan, I.; Omar, A.; Kristensen, T. ICOS OTC SOOP Release from G.O. Sars, 2025-12-06–2025-12-17, 2025. https://hdl.handle.net/11676/PJYEFd2h6AvRt3weOznuj0hH.

(6) Davies, E. J.; Nepstad, R. In Situ Characterisation of Complex Suspended Particulates Surrounding an Active Submarine Tailings Placement Site in a Norwegian Fjord. *Reg. Stud. Mar. Sci.* **2017**, *16*, 198–207. https://doi.org/10.1016/j.rsma.2017.09.008.

(7) Nepstad, R.; Liste, M.; Alver, M. O.; Nordam, T.; Davies, E.; Glette, T. High-Resolution Numerical Modelling of a Marine Mine Tailings Discharge in Western Norway. *Reg. Stud. Mar. Sci.* **2020**, *39*, 101404. https://doi.org/10.1016/j.rsma.2020.101404.

(8) Parkhurst, D. L.; Appelo, C. A. J. *Description of Input and Examples for PHREEQC Version 3: A Computer Program for Speciation, Batch-Reaction, One-Dimensional Transport, and Inverse Geochemical Calculations*; USGS Techniques and Methods 6-A43; U.S. Geological Survey, 2013. https://doi.org/10.3133/tm6A43.

(9) Baeten, N. J.; Lepland, A.; Bøe, R.; Amundsen, A.; Chand, S.; Longva, O. Distribution, Deposition and Impact of Submarine Mine Tailings Disposal on the Fjord Bottom in Frænfjorden, Western Norway. *Nor. J. Geol.* **2020**, *100* (1), 1–24. https://doi.org/10.17850/njg100-1-3.

(10) Lunstrum, A.; Berelson, W. CaCO3 Dissolution in Carbonate-Poor Shelf Sands Increases with Ocean Acidification and Porewater Residence Time. *Geochim. Cosmochim. Acta* **2022**, *329*, 168–184. https://doi.org/10.1016/j.gca.2022.04.031.

(11) Trannum, H. C.; Gundersen, H.; Escudero-Oñate, C.; Johansen, J. T.; Schaanning, M. T. Effects of Submarine Mine Tailings on Macrobenthic Community Structure and

Ecosystem Processes. *Sci. Total Environ.* **2018**, *630*, 189–202. https://doi.org/10.1016/j.scitotenv.2018.02.207.

(12) Trannum, H. C.; Borgersen, G.; Oug, E.; Glette, T.; Brooks, L.; Ramirez-Llodra, E. Epifaunal and Infaunal Responses to Submarine Mine Tailings in a Norwegian Fjord. *Mar. Pollut. Bull.* **2019**, *149*, 110560. https://doi.org/10.1016/j.marpolbul.2019.110560.

(13) Wetzel, R. G. *Limnology: Lake and River Ecosystems*, 3rd ed.; Academic Press, 2001.

(14) Dodds, W. K.; Smith, V. H. Nitrogen, Phosphorus, and Eutrophication in Streams. *Inland Waters* **2016**, *6* (2), 155–164. https://doi.org/10.5268/IW-6.2.909.

(15) Emerson, K.; Russo, R. C.; Lund, R. E.; Thurston, R. V. Aqueous Ammonia Equilibrium Calculations: Effect of pH and Temperature. *J. Fish. Res. Board Can.* **1975**, *32* (12), 2379–2383. https://doi.org/10.1139/f75-274.

(16) U.S. Environmental Protection Agency. *Aquatic Life Ambient Water Quality Criteria for Ammonia—Freshwater 2013*; EPA 822-R-13-001; U.S. Environmental Protection Agency, 2013.

(17) Reynolds, C. S. *The Ecology of Phytoplankton*; Cambridge University Press, 2006. https://doi.org/10.1017/CBO9780511542145.